Experimental implementation of a catalytic membrane reactor for the direct synthesis of DME from H_2+CO/CO_2

Pablo Rodriguez-Vega[a], Ainara Ateka[a]*, Izumi Kumakiri[b], Hector Vicente[a], Javier Ereña[a], Andres T. Aguayo[a], Javier Bilbao[a]

[a] Department of Chemical Engineering, University of the Basque Country UPV/EHU, P.O. Box 644, 48080 Bilbao, Spain

[b] Graduate School of Science and Technology for Innovation, Graduate School Science and Engineering, Yamaguchi University, Ube, 755-8611, Japan

*Corresponding author. Tel.: 34-94-6015361. E-mail address: ainara.ateka@ehu.eus

Abstract

The direct synthesis of dimethyl ether (DME) by the hydrogenation of CO_2 and CO_2/CO_x mixtures has been studied in an original packed bed membrane reactor (PBMR). The role of the hydrophilic LTA zeolite membrane is to remove H_2O from the reaction medium, reducing therefore the thermodynamic limitations of methanol synthesis and dehydration stages. LTA zeolite has the best permeation properties among the studied zeolites (LTX and SOD). The experiments were carried out using a CuO-ZnO-ZrO_2/SAPO-11 catalyst at 275-325 ºC, 10-40 bar, space time of 10 g_{cat} h $(mol_C)^{-1}$ and using in the permeate section a sweeping gas flowrate of the same composition as that fed to the reaction section. The results (DME yield, CO_2 conversion and product distribution) of the PBMR are compared with those obtained in PBR without membrane. In the hydrogenation of CO_2, a DME yield of 12 % and a CO_2 conversion of 20 % are obtained at 275 ºC, 40 bar and space time of 10 g_{cat} h $(mol_C)^{-1}$ with a great catalyst stability.

Keywords: dimethyl ether, CO_2, syngas, membrane reactor, LTA zeolite, deactivation

1. Introduction

The utilization of a membrane in catalytic process reactors pursues reducing both energy consumption and production costs, as well as minimizing the environmental impact. This strategy is part of the engineering approaches for process intensification and has a growing implantation in fuels and chemical products synthesis processes from sustainable sources (N Diban et al., 2013; Cannilla et al., 2017; Tian et al., 2018). Among these processes, the direct synthesis of dimethyl ether (DME) is considered one of the most attractive routes for the large scale CO_2 valorization (Olah et al., 2009; Rafiee et al., 2018; Leonzio, 2018). DME has upward commercial interest as automotive and domestic fuel (has a cetane number of 56) (Arcoumanis et al., 2008; Semelsberger et al., 2006) and as reactant (alternative to methanol) for the production of raw chemicals (olefins and aromatics) (Pérez-Uriarte et al., 2016; Cordero-Lanzac et al., 2018) and the production of H_2 in vehicles (through steam reforming) (Shimoda et al., 2011; Oar-Arteta et al., 2016). It is also widely used as refrigerant and spray (Good and Francisco, 2003), and in oil extraction (Javanmard et al., 2019). The reaction system for its direct synthesis from CO and CO_2 hydrogenation involves:

Methanol synthesis:	$CO + 2H_2 \leftrightarrow CH_3OH$	(1)
	$CO_2 + 3H_2 \leftrightarrow CH_3OH + H_2O$	(2)
Reverse water gas shift (rWGS):	$CO_2 + H_2 \leftrightarrow CO + H_2O$	(3)
Methanol dehydration to DME:	$2CH_3OH \leftrightarrow CH_3OCH_3 + H_2O$	(4)
Hydrocarbons formation (undesired):	$CO + 3H_2 \leftrightarrow CH_4 + H_2O$	(5)

Using bifunctional catalysts, methanol synthesis and WGS reactions are catalyzed by the metallic function, while methanol dehydration by the acid function. Performing

methanol dehydration *in situ* in the same reactor displaces the thermodynamic equilibrium of the methanol synthesis reactions. The thermodynamic advantages over methanol synthesis and the synthesis of DME in two separate reaction stages (methanol synthesis and its dehydration) have been quantified in the literature, and are particularly interesting to favor CO_2 conversion when co-fed with syngas (Chen et al., 2016; Ateka et al., 2017).

Catalyst preparation has received great attention (Sun et al., 2014; Catizzone et al., 2018; Mondal and Yadav, 2019), in particular, seeking to promote CO_2 conversion and improve stability. The most studied metallic function is CuO-ZnO-Al_2O_3 with different metallic oxides such as MgO, CeO_2, MnO or ZrO_2 among others and their well-established behavior in the synthesis of methanol is reported. The metallic oxides were used to replace Al_2O_3 partially or totally or as promoters to increase the stability of Cu, attenuating its sintering (Frusteri et al., 2015; Bonura et al., 2016; Zhou et al., 2016). The conventional acid function used for methanol dehydration (γ-Al_2O_3) has been progressively replaced by less hydrophilic materials, such as some zeolites (HZSM-5 and ferrierite have been widely studied) (García-Trenco and Martínez, 2012; Cai et al., 2016; Frusteri et al., 2017) and silicoaluminophosphates (SAPOs), as SAPO-18 and SAPO-11 (Ateka et al., 2016, 2017). These acidic functions must have a high density of sites, but of moderate acidic strength to minimize the formation of coke. The conventional preparation method of bifunctional catalysts consists of physically mixing both functions (hybrid catalysts), and subsequent pelletizing to achieve an adequate particle size and the required mechanical resistance for its use in the reactor. As to the core-shell configuration of the particles regards, even if it can avoid negative effects resulting from the contact between the metallic and acid functions (García-Trenco et al., 2012; Bonura et al., 2020), the preparation method has greater difficulties than those of

the hybrid catalyst (Sánchez-Contador et al., 2018a). Considering the reaction system for the direct synthesis of DME (Eqs. (1)-(5)), the presence of H_2O in the reaction medium conditions the thermodynamics of the process, limiting the conversion of CO and CO_2 yielding DME. Consequently, the proposal of a hydrophilic membrane reactor that favors the separation of H_2O from the medium is a challenge of relevant interest. Iliuta et al. (2010, 2011) have studied by simulation the removal of H_2O from the reaction medium using a hydrophilic membrane or by means of adsorption in order to increase methanol and DME yields. Diban et al. (2013) have proposed a mathematical model to simulate an isothermal packed bed membrane reactor system, in order to determine the transport characteristics of the most suitable membrane for the direct synthesis of DME, co-feeding CO_2 together with CO and H_2. In this model unidirectional flow of the feed and the sweeping gas in counter-current mode are considered. These authors emphasize the need of a stable hydrophilic membrane (ZSM-5, MOR, SIL) as those used for Fischer-Tropsch (FT) synthesis. They also pointed out the restrictions of H_2O permeation selectivity at high reaction temperatures. Using for the simulation an ideal membrane (impermeable to methanol and DME) these authors (Diban et al., 2014) achieved an upgrade of DME yield of over 30 %, compared to that obtained without a membrane. Farsi et al. (2016) have compared, by simulation of a nonisothermal one-dimensional reactor, the performance for the direct synthesis of DME of a double membrane reactor (hydrogen-water), previously proposed for methanol synthesis (Farsi and Jahanmiri, 2012), with that of other reactors with hydrophilic membranes, hydrogen selective membranes and without membrane. De Falco et al. (2016) have demonstrated by simulation the advantages of two alternative reaction systems, thus, a zeolite membrane reactor and two series units, which consisted of a packed bed reactor and a water separation module. Subsequently, these authors (De

Falco et al., 2017a) have studied the effect of the operation conditions (CO_2/CO_x and H_2/CO_x ratios in the feed, temperature, pressure, space time) on CO_2 conversion and DME yield, at industrial scale conditions with a non-isothermal model in the simulation of the membrane reactor. Among the simulation results, the achievement of the following results is to be highlighted: a DME yield of 0.75 (0.57 in the conventional reactor), a DME selectivity close to 100 % and CO_x and CO_2 conversions of 0.75 and 0.69, respectively, enhancing in 15.4 % and 30.2 % the results in the conventional reactor. Additionally, the results have been improved by these authors (De Falco et al., 2017b), with an operation strategy called Double Recycling Loop DME (DRL-DME). This design consists of the utilization of a pure CO_2 stream as sweeping gas in the permeation zone and recirculation to the reactor.

Despite the advances in the preparation of zeolite membranes and in their application to membrane reactors in different catalytic processes (Bedard and Liu, 2018), the application of this type of membranes in methanol and DME synthesis is still at the preliminary stage, consisting of the proposal of H_2O perm-selective membranes to be used in severe reaction conditions (Gallucci, 2018). Galluci et al. (2004) have experimentally upgraded the yield of methanol synthesis using a LTA membrane, and Fedosov et al. (2015) have used a LTA membrane (NaA Zeolite) for the dehydration of methanol towards DME. Gorbe et. al. (2018) have obtained results on the capacity of A zeolite to selectively separate water and methanol. The experiments have been carried out measuring the permeation of a H_2, CO_2 and H_2O mixture, within the range of interest for methanol synthesis (160-240 ºC, 10-27 bar). Recently, Lee et al. (2021) have used a polyimide hollow fiber membrane reactor for methanol synthesis.

In this work, a laboratory scale packed bed reactor provided with a LTA zeolite membrane (selected from a group of materials according to its permselectivity) has been

used in the direct synthesis of DME. The study has been conducted in a wide range of operating conditions, analyzing the effects of reaction temperature, pressure and CO_2/CO_x ratio in the feed on various reaction indices (DME and methanol yield and selectivity, CO_x conversion and CO_2 conversion) and on the stability of the catalyst. The experimental results are compared with those obtained in a reactor without membrane to quantify the shift attained in the yield of DME and the conversion of CO_2 over the thermodynamic limitations. The composition of the used catalyst (CuO-ZnO-ZrO_2/SAPO-11) has been optimized in previous works (Sánchez-Contador et al., 2018a, 2018b, 2018c).

2. Experimental

2.1. Catalyst preparation and characterization

CuO-ZnO-ZrO_2/SAPO-11 catalyst was prepared by physical mixture and subsequent pelletizing of the metallic and acid functions in a 1/2 mass ratio. The atomic Cu:Zn:Zr ratio of the metallic function (determined by ICP-OES analysis) is 2:0.75:1.21. The suitability of this composition and the preparation conditions for each of the functions have been established in previous works (Sánchez-Contador et al., 2018a, 2018b, 2018c). Likewise, the characterization methodologies for each of the functions comprising the catalyst and the bifunctional catalyst have been described in detail in these works. The most significant physico-chemical properties of the final catalyst are listed in Table 1.

Table 1. Physico-chemical properties of the CuO-ZnO-ZrO_2/SAPO-11 bifunctional catalyst.

Physical properties			
S_{BET} ($m^2\,g^{-1}$)	V_{micro} ($cm^3\,g^{-1}$)	V_{meso} ($cm^3\,g^{-1}$)	d_p (Å)
122	0.029	0.170	97.9

Metallic properties		
S_{Cu} ($m^2\,g_{Cu}^{-1}$)	S'_{Cu} ($m^2\,g_{cat}^{-1}$)	Cu dispersion (%)
53.5	6.3	8.2

Acid properties	
Total acidity ($mmol_{NH3}\,g^{-1}$)	Acid strength (kJ mol_{NH3}^{-1})
0.17	85

2.2. Membrane preparation and characterization

Three types of microporous zeolite membranes, thus, Linde Type A (LTA), Linde Type X (LTX) and Sodalite (SOD) membranes were synthesized on stainless steel supports purchased from Mott Corporation. Table 2 shows the syntheses temperatures and times for the different membranes. The preparation conditions and materials are detailed in the Appendix (Tables A4-A6).

Table 2. Hydrothermal conditions for the synthesis of the different membranes.

Zeolite membrane	Temperature (ºC)	Time (h)
Linde type A (LTA)	110	12
Linde type X (LTX)	90	8
Sodalite (SOD)	130	48

The morphology of the membranes was analyzed by scanning electron microscopy (SEM, in a JEOL/JSM-7000f equipment, equipped with a W filament, 3.5 eV resolution, attached to energy dispersive X-ray analyzer EDX, Oxford, 133 eV resolution).

Pervaporation and vapor permeation were performed to examine the dehydration performances of the membranes. The pervaporation (PV) of the different membranes was evaluated as described in the Appendix. The separation factors (Eqs. (A1) and (A2)) and fluxes (Eq. (A3)) of the PV experiments were calculated for EtOH/H_2O and MeOH/H_2O mixtures at 75 ºC and 60 ºC, respectively.

In addition, permeation of different gases (He, H_2, CO_2 N_2, CH_4 and SF_6) was measured at 100-200 ºC. Ideal selectivity was calculated from the permeation ratio of two gases. Thermal stability tests were performed by characterizing the membranes before and after thermally treating the membranes at 300 ºC with PV, VP, XRD and SEM. The temperature of the thermal treatment represents the DME synthesis temperature.

The used techniques and analysis conditions have been described in the Appendix (section A3).

2.3. Packed bed membrane reactor (PBMR)

The stainless steel packed bed membrane reactor (PBMR), shown in Fig. 1, structurally presents two concentric sections: the reaction section, in which the catalytic bed is located, surrounded by another concentric system that allows the sweep of the permeate flow (permeate section).

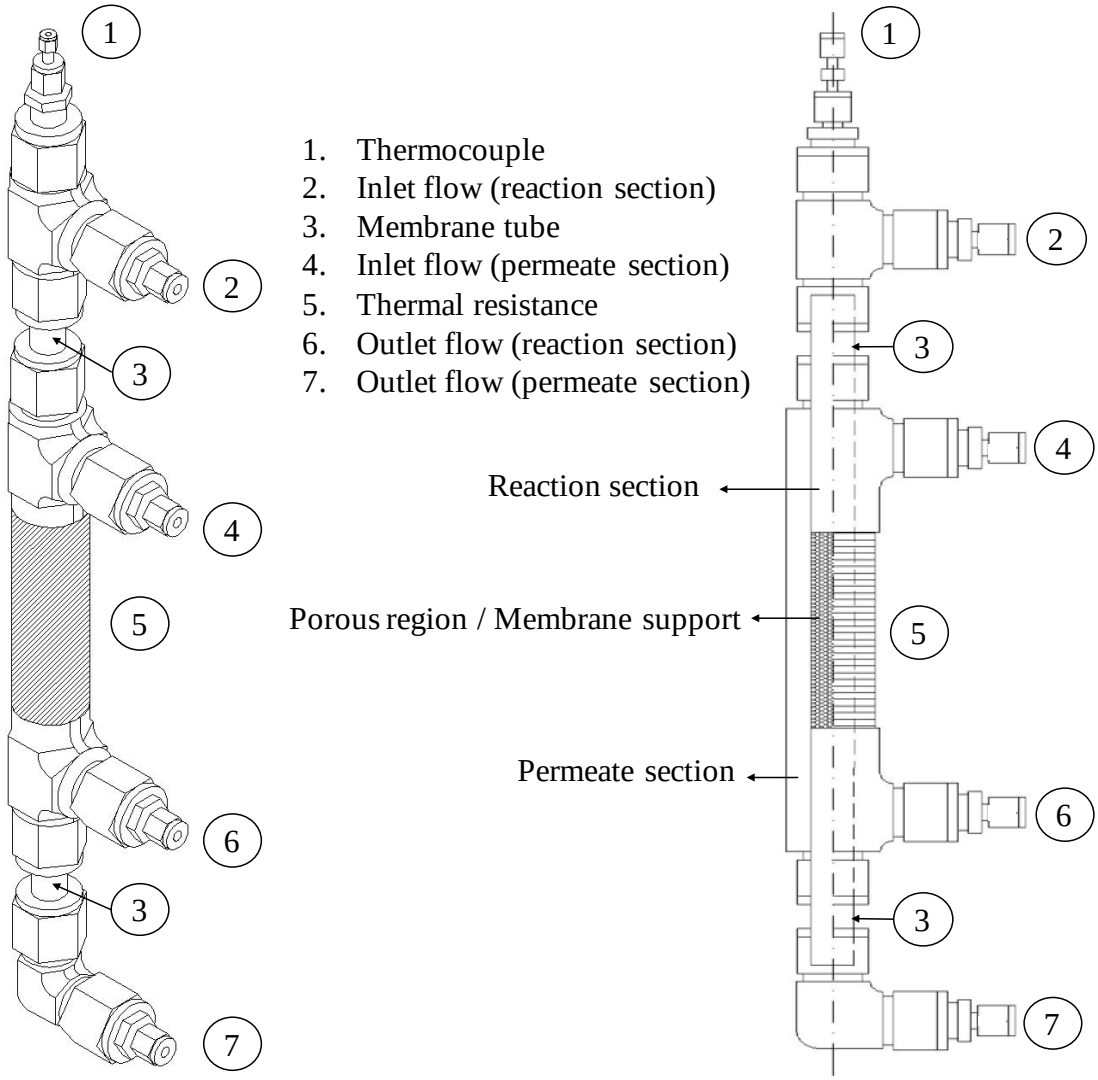

Fig. 1.Configuration of the packed bed membrane reactor (PBMR).

The reaction section is limited by the stainless steel membrane tube (Mott Corporation). The inner diameter of the stainless steel tube is 9.5 mm and its length, 240 mm. It has a central region of 70 mm, that corresponds to the catalytic bed, and its outer surface permits the permeation of water vapor from the reaction medium towards the permeate section. The catalytic bed is composed by a mixture of catalyst and solid inert, carborundum (CSi) with an average particle diameter > 0.5 mm, as to obtain a sufficient bed length in order to ensure a proper distribution of the gas through it and isothermal condition when operating with moderate space time values. In Fig. 2, a schematic

diagram of the conceptual design is depicted, where the composition of the gases entering and exiting the reaction and permeation sections can be observed, along with the H_2O permeation strategy.

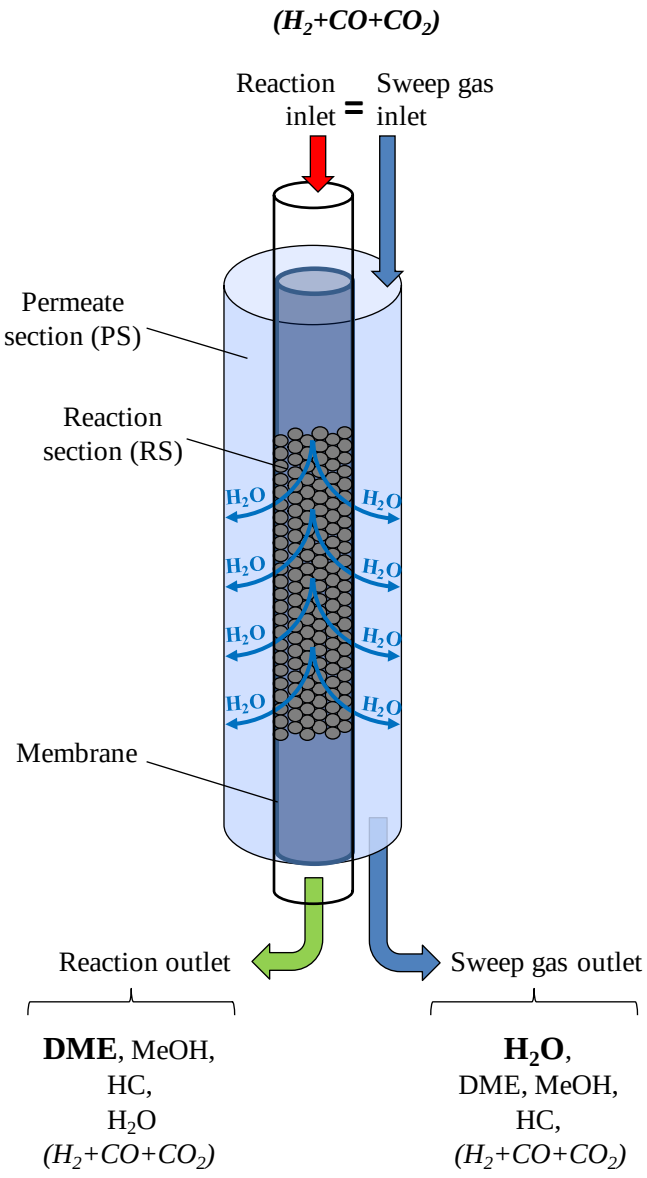

Fig. 2. Diagram of the circulation of the components in the PBMR.

2.4. Reactor tests

The membrane reactor system (Fig. A1) has been designed, built up and put into operation through the appropriate adjustment of a commercial equipment for catalytic reactions (Microactivity Reference from PID Eng&Tech., Madrid, Spain). Two sets of mass flow controllers (Bronkhorst High-Tech B.V. Series) regulate the flow rate of the feed gas mixtures and the sweep gas, respectively. The feed gases used are N_2 (inert gas), He (carrier gas towards the gas chromatograph, Agilent 490) and the reactive gases H_2, CO_2, CO/CO_2 and synthesis gas (H_2/CO). The same sweeping strategy was used for the whole set of experiments. Hence, the sweeping gas in the permeate section was fed with the same composition as in the reaction section (total flow rate of 60 cm^3 min^{-1} of H_2+CO/CO_2).

The temperature was controlled and monitored by TOHO TTM-005 controllers with K-Type thermocouples at two points. One of them is placed in the catalytic bed within the reactor tube controlling the surrounding thermal resistance, and the other is located in the hot box of the reactor system. Additionally, there was a heating system surrounding the outlet flow of gases, in order to avoid any condensation before entering the gas chromatograph. The typical reaction temperature studied was 275-325 ºC.

Two transducers (Sensor-Technik-Wiedemann GmbH) were used to control the pressure of the system. They act simultaneously on two needle pressure valves, placed at the reactor outlet, which regulate the pressure in both sections. The reaction feed gases pass through a 6-port valve to determine if they are addressed towards either the gas chromatograph or to the gas exit (bypass connected), or enter the reactor (bypass disconnected). The packed bed membrane reactor (PBMR) system, in comparison with a packed bed reactor (PBR), requires a second bypass valve within it to regulate

whether the reaction or the permeate section will be analyzed. Once the reaction has taken place, a small part of the reaction and permeate fluxes (around 1 cm^3) are diluted in a He stream and sent to the gas chromatograph to be analyzed continuously on-line every 2.5 min.

The PBMR system is equipped with a process control software (Process@), which allows to handle and program the operating conditions by creating automatic sessions varying feed, pressure and temperature, among others. The reaction products are analyzed on-line in a gas micro-chromatograph (micro-GC Agilent 490), equipped with fixed injectors and TCD detectors implemented in two analytic modules. Each module is provided by one of the following columns: Molecular sieve (MS-5): (10 m x 12 mm) where H_2, O_2, N_2 and CO are analyzed; Porapak Q (PPQ): (10 m x 20 mm) where CH_4, CO_2, ethane, H_2O, propane, methanol and DME are analyzed. In Table A1 the analysis conditions corresponding to each GC-module are listed. In order to identify and quantify properly the reaction products from both the reaction and permeate sections, periodic calibrations of the micro-GC have been performed using pattern compounds bottles and known gas composition mixtures. The surface of each chromatographic peak is proportional to the molar quantity of the compound present in the sample, taking into account the calibrated specific response factors of the area of each compound (Table A2). The acquisition and processing of the data are carried out by the Star Toolbar. This software allows knowing the molar fraction of the sample, and so, calculating the reaction indices (products yield and selectivity and reactants conversion).

The results have been quantified according to the following reaction indices: 1) yield of each product; 2) CO_2 valorization; 3) CO_x (that is, $CO+CO_2$) conversion, and; 4) selectivity of each product. The yield of each *i* product (Y_i) is defined by the ratio between its molar flow rate and the molar flow rate of COx in the feed:

$$Y_i = \frac{n_i \cdot F_i}{F^0_{CO_x}} \cdot 100 \quad (6)$$

being n_i the number of carbon atoms of each *i* product; F_i, the molar flow rate of *i* product at the reactor outlet and $F^0_{CO_x}$ the molar flow rate of CO_x in the feed, respectively. It has to be considered that at the outlet of a PBMR two different flows are analyzed (reaction and permeate sections). Therefore, products yields in both reaction (RS) and permeate (PS) sections are summed in order to define a total yield (Y_T).

$$Y_{iT} = (Y_i)_{RS} + (Y_i)_{PS} \quad (7)$$

being $(Y_i)_{RS}$ and $(Y_i)_{PS}$ calculated from Eq. (6)

The conversion of CO_2 is defined by the expression:

$$X_{CO_2} = \frac{F^0_{CO_2} - F_{CO_2}}{F^0_{CO_2}} \cdot 100 \quad (8)$$

where F_{CO_2} is the molar flow rate of CO_2 at the reactor outlet. This conversion is directly related with the capability of valorizing CO_2 of each reactor configuration.

Moreover, the conversion of CO_x is defined by the ratio between the moles of CO and CO_2 in the feed that have been converted:

$$X_{CO_x} = \frac{F^0_{CO_x} - F_{CO_x}}{F^0_{CO_x}} \cdot 100 \quad (9)$$

being F_{CO_x} the molar flow rate of ($CO+CO_2$) at the outlet of the reactor.

The selectivity (S_i) represents the ratio between the molar flow rate of each *i* compound in the product flow (F_i) and the total molar flow of products (organic compounds, DME, methanol and paraffins), based on C units:

$$S_i = \frac{n_i \cdot F_i}{\sum_i (n_i \cdot F_i)} \cdot 100 \quad (10)$$

Like in the yield calculation (Eq. (7)), products selectivities in both reaction and permeate sections are summed in order to define a total selectivity (S_{iT}).

$$S_{iT} = (S_i)_{RS} + (S_i)_{PS} \quad (11)$$

3. Results and discussion

3.1. Membrane selection

In Table 3 the PV performances of the synthesized membranes are summarized. LTA membrane showed the best dehydration performance as it could be expected attending to the combination of this zeolites properties, thus, the Si/Al ratio (of 1, indicative of its hydrophilic nature (Osatiashtiani et al., 2017; Perez-Carbajo et al., 2020)) and structure (channels with a maximum diffusion diameter of 4.21 Å (Database of Zeolite Structures). As a result, a separation factor (α) for EtOH/H_2O and MeOH/H_2O mixtures higher than 9000 and 1400 were attained with LTA, respectively. Conversely, LTX and SOD membranes showed lower selectivity towards both mixtures, being α below 10. Another advantage of LTA membrane is the high reproducibility with a relatively simple synthesis method described in the Appendix (section A3). As the high dehydration performance is a key factor in the direct DME synthesis process, further tests were performed with the LTA membrane.

Table 3. Results of H_2O pervaporation from EtOH /H_2O and MeOH/H_2O mixtures through the different membranes at 75 ºC and 60 ºC, respectively.

Membrane	Composition	Feed (wt%)	Permeate (wt%)	Q (kg m^{-2} h^{-1})	α
LTA	EtOH H_2O	90 10	0.15 99.8	1.59	9329
LTA	MeOH H_2O	90 10	0.45 99.5	0.92	1486
LTX	EtOH H_2O	90 10	55.4 44.6	2.40	7.9
LTX	MeOH H_2O	90 10	69.4 30.6	2.00	2.9
SOD	EtOH H_2O	90 10	89.7 10.3	0.80	1.1

3.2. Membrane morphology

Physical and morphological properties. The porous texture of the LTA zeolite powder has been characterized by CO_2 adsorption at 0 ºC (in ASAP 2020 equipment, Micromeritics) (Fig. (A3)). To carry out the analysis, LTA has been prepared following the same procedure described in the Appendix, without introducing the metallic support in the autoclave. Well-defined CO_2 adsorption isotherm has been obtained with a practically saturated shape in the range of low relative pressure. Pore width and micropore surface, calculated using the Dubinin-Radushkevich equation and by the Horvath-Kawazoe method, are 3.98 Å and 458 m^2 g^{-1}, respectively. These results suggest that the crystalline zeolite presents narrow micropores (3.98 Å).

Structural properties. X ray diffraction (XRD) measurements have been used to study the crystallinity and purity of the LTA membrane. From the XRD pattern of the LTA membrane (Fig. 3) it can be confirmed, on one hand, that the zeolite has been appropriately synthesized (Belviso et al., 2018) and, on the other hand, its correct

crystallization on the stainless steel support (fundamental step within the membrane reactor configuration). Neat and well-defined peaks can be observed, indicating an absence of amorphous phase in the material. According to the database, the most intense peaks on the diffractogram clearly identified in Fig. 3 suggest that a crystalline phase with high purity supported on stainless steel can be achieved through this preparation method. The XRD pattern of steel can also be observed in Fig. 3, consisting of three peaks at higher values of 2θ angles (67.1, 79.5 and 129.1 degrees) attributed to the metallic support of the membrane (obtained in a PAN analytical Xpert Pro device).

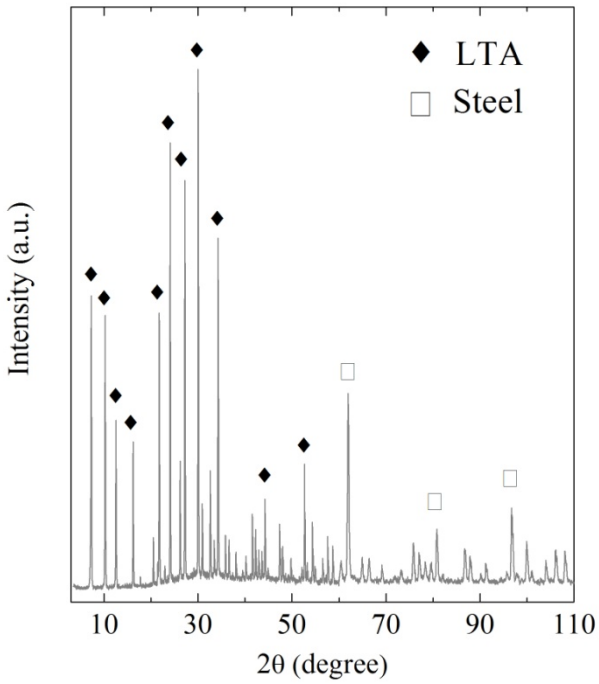

Fig. 3. XRD pattern of the synthesized LTA zeolite crystallized on stainless-steel support.

In Fig. 4 SEM micrographs of the synthesized LTA zeolite are depicted. At the front view of the membrane cross-section (Fig. 4a) both phases (zeolite and support) are clearly differentiated. A zeolite layer of regular thickness has been deposited on the surface of the non-polished stainless steel support. The homogeneous texture of the

LTA membrane (Fig. 4b) suggests a high effectiveness of the preparation method for the purpose of achieving a complete coverage of the support with zeolite crystals, in accordance with that reported by Belviso et al. (2018). As it is observed in Fig. 4c LTA zeolite morphology consists of cubic aggregates. SEM characterization has demonstrated the correct synthesis method of LTA membranes, highlighting the formation of uniform thickness zeolite layer and its homogeneous distribution on the support surface.

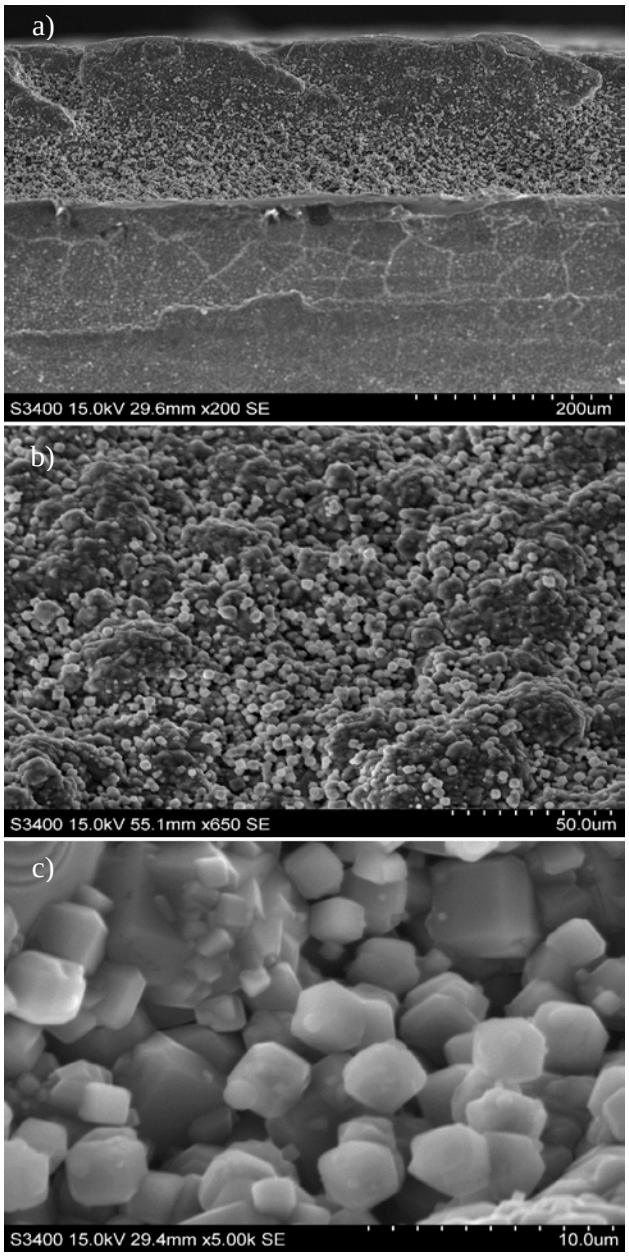

Fig. 4. SEM images of the LTA zeolite membrane. Cross-section (a) and top view at different scales (b and c).

3.3. Stability of LTA membrane

Pervaporation. The PV properties of the LTA membrane after its thermal treatment are shown in Table 4. Comparing with the results prior to the thermal treatment (Table 3) the separation factors (α), both for EtOH/H_2O and MeOH/H_2O mixtures, decrease after the treatment (2905 and 1011 respectively). Nevertheless, it maintains its hydrophilicity

towards both mixtures. Concerning the fluxes (*Q*) of the two feed compositions through the membrane, they are slightly raised from 1.59 to 1.70 kg m^{-2} h^{-1} for EtOH/H_2O (≈ 6 %) and from 0.92 to 1.05 kg m^{-2} h^{-1} for MeOH/H_2O (≈ 14 %).

Table 4. EtOH/H_2O and MeOH/H_2O mixtures pervaporation results through the thermally treated LTA membrane at 75 ºC and 60 ºC, respectively.

Composition	Feed (wt%)	Permeate (wt%)	*Q* (kg m^{-2} h^{-1})	α
EtOH	90	0.47	1.70	2905
H_2O	10	99.5		
MeOH	90	0.75	1.05	1011
H_2O	10	99.2		

Vapor permeation. VP performance of the LTA membrane after its thermal treatment is summarized in Table 5. LTA membrane H_2O permselectivity remains after its treatment (higher than 3000) and the vapor flux through it rises up to 1.32 kg m^{-2} h^{-1}.

Table 5. EtOH/H_2O mixture vapor permeation results through the thermally treated LTA membrane at 125 ºC.

Composition	Feed (wt%)	Permeate (wt%)	*Q* (kg m^{-2} h^{-1})	α
EtOH	90	0.19	1.32	3232
H_2O	10	99.8		

Single gas permeation. The permeances for different gases at different temperatures (100, 150 and 200 ºC) through the thermally treated LTA membrane are shown in Table 6. Moreover, in Table 7 the ideal selectivities of different gases at 100, 150 and 200 ºC through the thermally treated LTA membrane have been gathered. Increasing temperature up to 200 ºC, a slight increment in the gas permeances through the

thermally treated LTA membrane is observed. In spite of this permeance increase, the analysis demonstrates that even at high temperatures, the LTA membrane has low gas permeability and, therefore, is able to operate at temperatures near to those required in the synthesis of DME.

Table 6. Gas permeances through the thermally treated LTA membrane at 100, 150 and 200 ºC (in 10^{-9} mol m^{-2} s^{-1} Pa^{-1}).

Temperature (ºC)	He	H_2	CO_2	N_2	CH_4	SF_6
100	2.39	2.90	0.56	0.78	0.93	0.31
150	3.47	4.60	0.94	1.24	1.61	0.55
200	9.24	13.2	3.18	3.61	4.34	1.66

Table 7. Ideal selectivities for different gas mixtures through thermally treated LTA membrane at 100, 150 and 200 ºC.

Temperature (ºC)	H_2/N_2	H_2/CH_4	CO_2/N_2	CO_2/CH_4	He/SF6	H_2/SF_6
100	3.7	3.1	0.3	0.2	10	11
150	3.7	2.8	0.8	0.6	6	8
200	3.7	3.0	0.9	0.7	6	8

Inert character. The null activity of the membrane in the reactions involved in the synthesis of DME (synthesis of methanol and its dehydration to DME) has been ascertained by means of experiments feeding syngas and co-feeding methanol with syngas, respectively. In both cases the conversion and the formation of paraffins and coke is null.

3.4. PBMR, Effect of reaction temperature

Fig. 5 shows an example of the evolution with time on stream (TOS) of the molar fractions of the reaction products (DME, MeOH, H_2O) at the reactor outlet in the

reaction section (RS) and in the permeate section (PS). These results, shown as an example, correspond to CO_2 hydrogenation at 275 ºC and 40 bar. Under these conditions, the advance of the reverse WGS reaction is facilitated, what leads to a high formation of H_2O. It should be noted that this is a key reaction for the production of DME since CO is more effective than CO_2 under these conditions (Aguayo et al., 2007; Ateka et al., 2018). The low concentrations of DME and methanol in the PS, show that the membrane is perm-selective towards these molecules (kinetic diameter of ca. 4.3 Å and 3.8 Å, respectively, and 2.6 Å for H_2O), specially for DME. In Fig. A2, the concentration values of all the gaseous components in the reaction and permeate sections are shown for different reaction temperature and different CO_2/CO_x ratios in the feed.

The similar H_2O concentration values in the reaction and permeation sections observed in Figs. 5 and A2 reveal a good degree of H_2O separation attained with the membrane. Nonetheless, the undesired partial permeation of methanol and DME also takes place. The high pressure and temperature required for this reaction have a great responsibility on limiting the permeation selectivity of H_2O with respect to oxygenates.

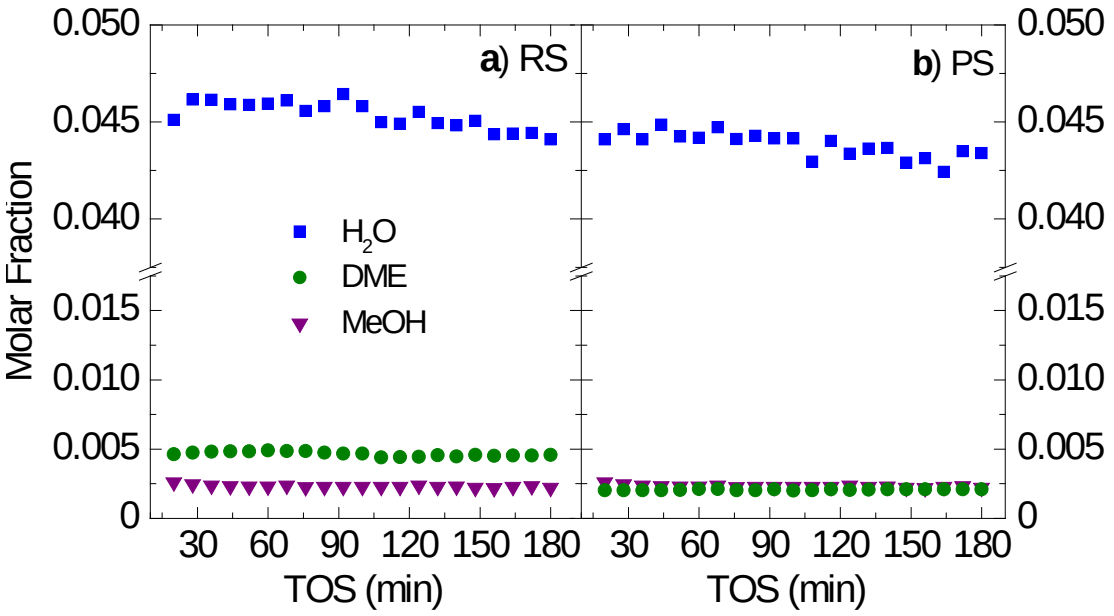

Fig. 5. Evolution of H_2O, DME and methanol molar fractions with time on stream. (a) results in the reaction section (RS) and (b) results in the permeate section (PS). Reaction conditions: 275 ºC; 40 bar; 10 g_{cat} h $(mol_C)^{-1}$; CO_2/CO_x, 1; H_2/CO_x, 3. Permeate conditions: equal composition and flow rate (60 cm^3 min^{-1}) as in the reaction section.

The common temperature range for DME synthesis studied in the literature is 250-300 ºC, since the temperature is limited by the thermodynamic equilibrium (Ateka et al., 2017) and also to preserve the hydrothermal stability of Cu in the catalyst. Nevertheless, the utilization of the membrane reactor (PBMR) diminishes the thermodynamic limitations, due to the lower H_2O concentration in the reaction medium, permitting the displacement of the thermodynamic equilibrium of H_2O formation reactions (methanol synthesis, reverse WGS and methanol dehydration). Consequently, it allows operating at higher temperatures achieving a higher conversion. Furthermore, the composition and conditions used for the preparation of the catalyst are adequate to confer an acceptable hydrothermal stability at 325 ºC. The fact that H_2O concentration in the reaction

medium is lower than in the conventional reactor (PBR) is, *a priori*, another advantage of the PBMR, in which less Cu sintering is expected. Attending to this advantage the studied temperature range has been 275-325 ºC.

Fig. 6 shows the effect of temperature in the different reaction indices at zero TOS (Figs. 6a,b) and on the stability of the catalyst (Fig. 6c) for certain reaction conditions (30 bar; 10 g_{cat} h $(mol_C)^{-1}$; CO_2/CO_x, 0.5; H_2/CO_x, 3) and H_2+CO/CO_2 feedstock. Fig. 6a shows that temperature has a great relevance on CO_x conversion, improving from 13.3 % at 275 ºC to 19.3 % at 325 ºC. DME yield enhances from 275 ºC until 300 ºC, achieving a maximum of 14.8 % at this temperature. Further increasing reaction temperature, a slight decay is observed due to, predictably, the thermodynamic limitation. However, CO_2 conversion is favored upon rising temperature, reaching 17.5 % at 325 ºC. MeOH and paraffins yields continue rising with a maximum of 3.7 % and 1.1 %, respectively, at 325 ºC.

As a consequence of the evolution of the individual yields with temperature, DME selectivity (Fig. 6b) drops when increasing temperature from 275 to 325 ºC, remaining quasi-constant at higher temperature. On the other hand, paraffins selectivity should be pointed out since it rises up to 5.6 % at 325 ºC. At this temperature, paraffins formation mechanisms are promoted, either from DME and methanol through the hydrocarbon pool mechanism (activated by the acid function) or through methanation or Fischer-Tropsch mechanisms from CO and CO_2 on the metallic function.

The formation of hydrocarbons facilitates deactivation by coke deposition, due to their role as intermediates for aromatics formation, which condensate to coke. The effect of temperature on the evolution of DME yield with time on stream (TOS) depicted in Fig. 6c demonstrates how temperature affects the stability of the catalyst, which is lower the

higher the temperature is within the range of 275-300 ºC. Nevertheless, at 325 ºC catalyst stability is greater than at 300 ºC, which can be related to catalyst sintering. The lower DME yield at 325 ºC than at 300 ºC, at zero time on stream, has therefore lower deactivation as favorable counterpart. It should also be pointed out that deactivation at 275 ºC is significantly slow.

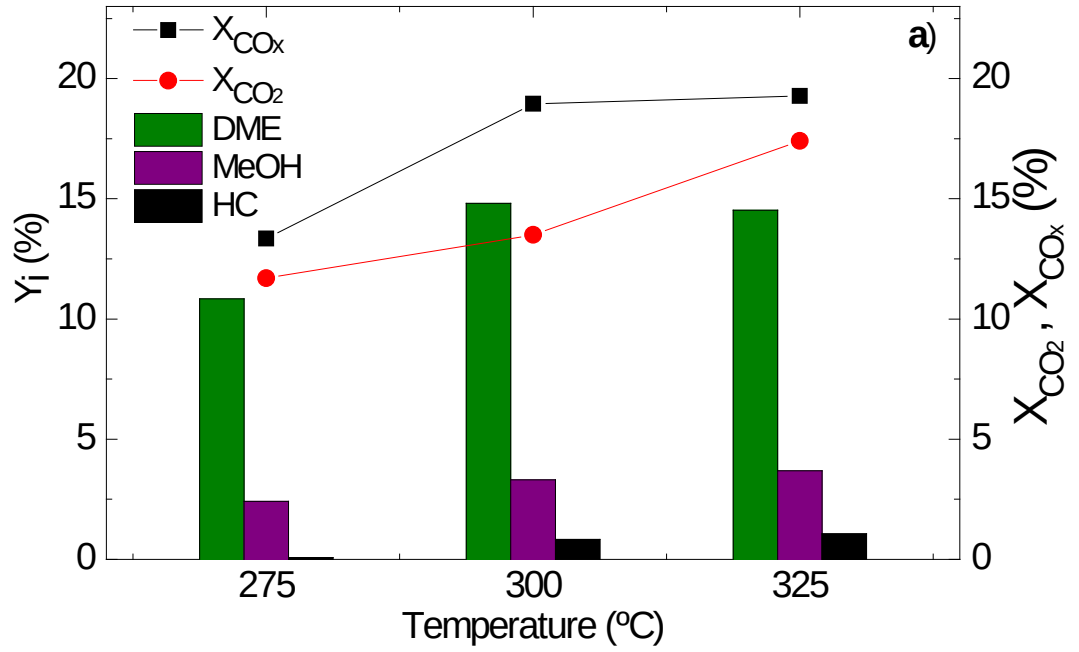

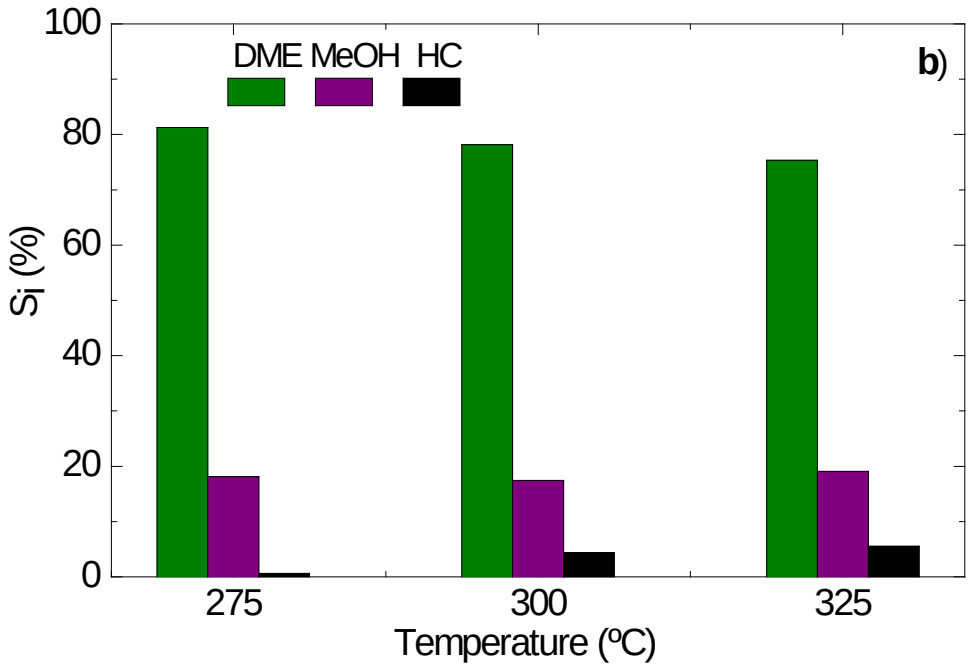

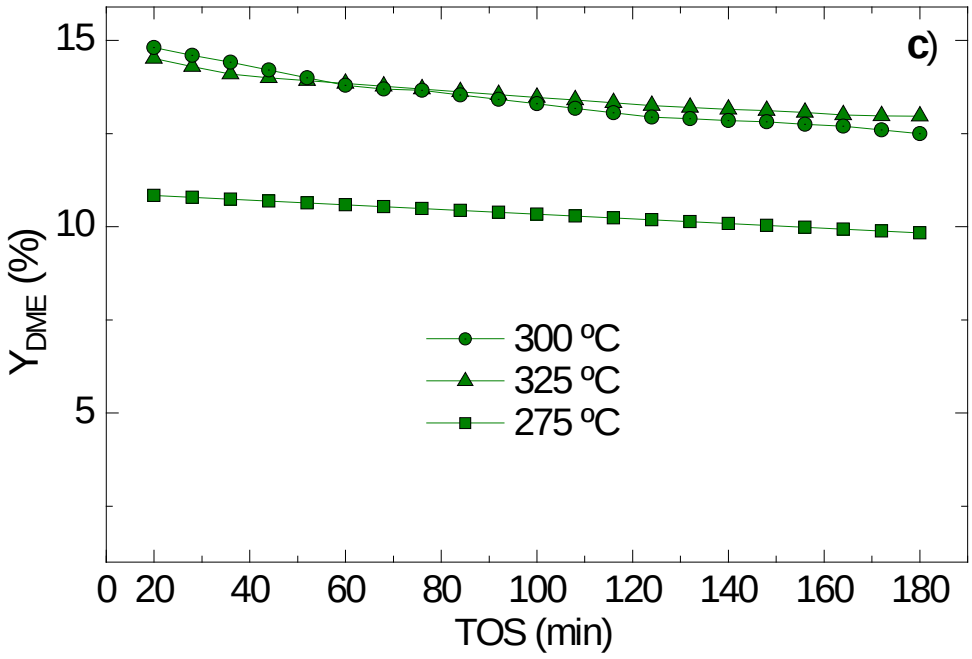

Fig. 6. Effect of reaction temperature on DME, MeOH and hydrocarbons yield, and CO_x and CO_2 conversion (a), on product selectivity (b) at zero time on stream; and the evolution of DME yield with time on stream (c) at different reaction temperatures. Reaction conditions: 30 bar; 10 g_{cat} h $(mol_C)^{-1}$; CO_2/CO_x, 0.5; H_2/CO_x, 3. Permeate conditions: equal composition and flow rate (60 cm^3 min^{-1}) as in the reaction section.

The influence of the feed composition was also studied. When a feed mixture of H_2+CO_2 was fed, the maximum CO_x conversion corresponds to the lowest temperature studied (275 ºC, 15.93 %), and decreases at higher temperatures (Fig. 7a). This tendency was different to that obtained with the H_2+CO/CO_2 feed as shown in Fig. 6. With regard to CO_2 conversion, on the contrary, it is upgraded by increasing temperature, achieving a value of 34.0 % at 325 ºC. This improvement in CO_2 conversion with temperature is due to the key role the reverse WGS reaction (Eq. (3)) plays, where CO_2 is converted to CO, more reactive for methanol synthesis. This remarkable effect is very

important in the process thermodynamics. Moreover, the greatest DME yield is obtained at 275 ºC (10.5 %), while methanol yield remains quasi-constant within the studied temperature range (4.3 %). In contrast, paraffins yield rises with temperature, reaching a peak of 0.4 % at 325 ºC.

The effect of reaction temperature on products selectivity is presented in Fig. 7b. Within the studied temperature range DME selectivity decreases from its maximum (70.2 % at 275 ºC) to 51.6 % at 325 ºC whereas that of MeOH rises by about 46 %. It should be emphasized that methanol is the main byproduct. This formed methanol is a minor issue for the industrial process scale-up, since it is a product of commercial interest itself, and it can also be dehydrated towards DME under atmospheric pressure in an independent reactor (Sierra et al., 2013). Paraffins selectivity increases significantly, from being barely detectable at 275 ºC to its maximum (4.5 %) at 325 ºC, which indicates, as previously described, that at this temperature paraffins formation mechanisms are activated.

The trend of the evolution of DME yield with TOS (Fig. 7c) at different temperatures (275-325 ºC) indicates that feeding CO_2 the deactivation of the catalyst seems to be imperceptible within this temperature range.

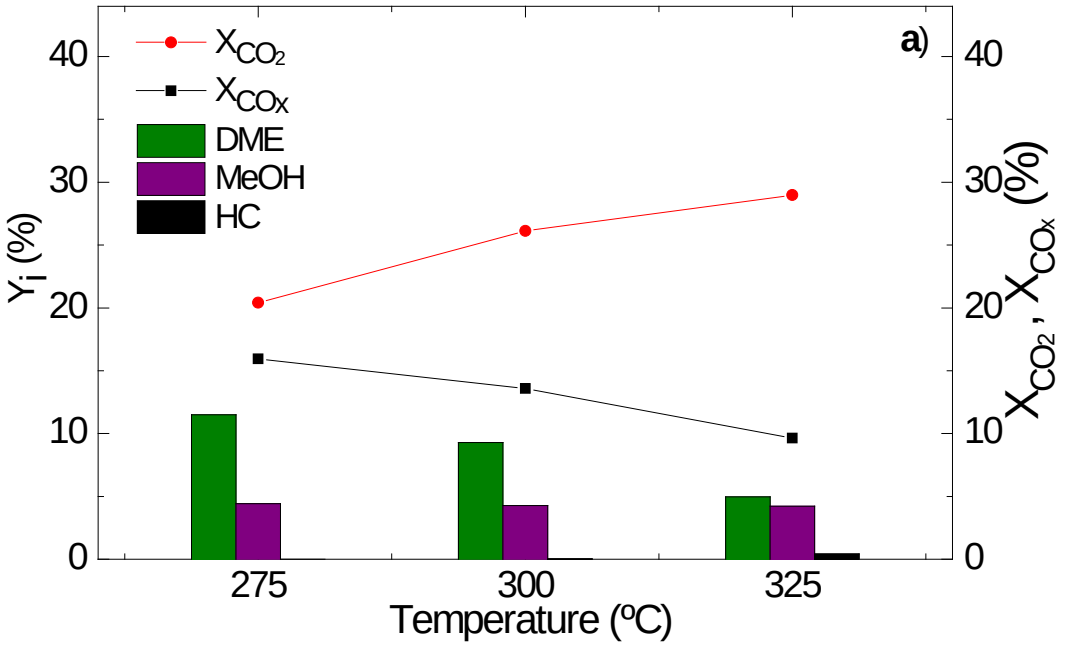
a)
X_{CO_2}
X_{COx}
DME
MeOH
HC
Y_i (%)
X_{CO_2}, X_{COx} (%)
0
10
20
30
40
275
300
325
Temperature (ºC)

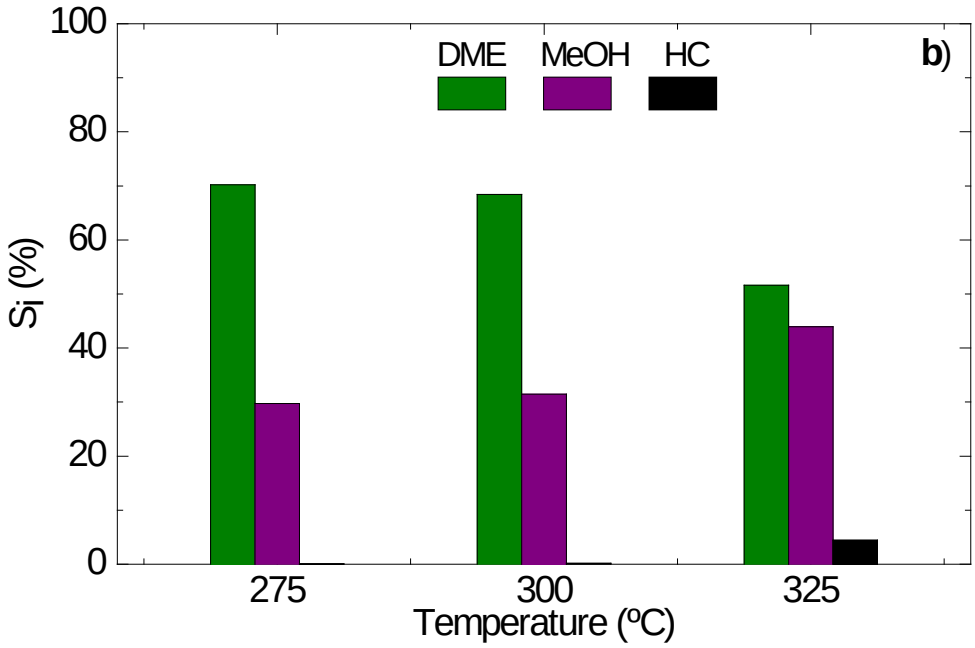
b)
DME
MeOH
HC
S_i (%)
0
20
40
60
80
100
275
300
325
Temperature (ºC)

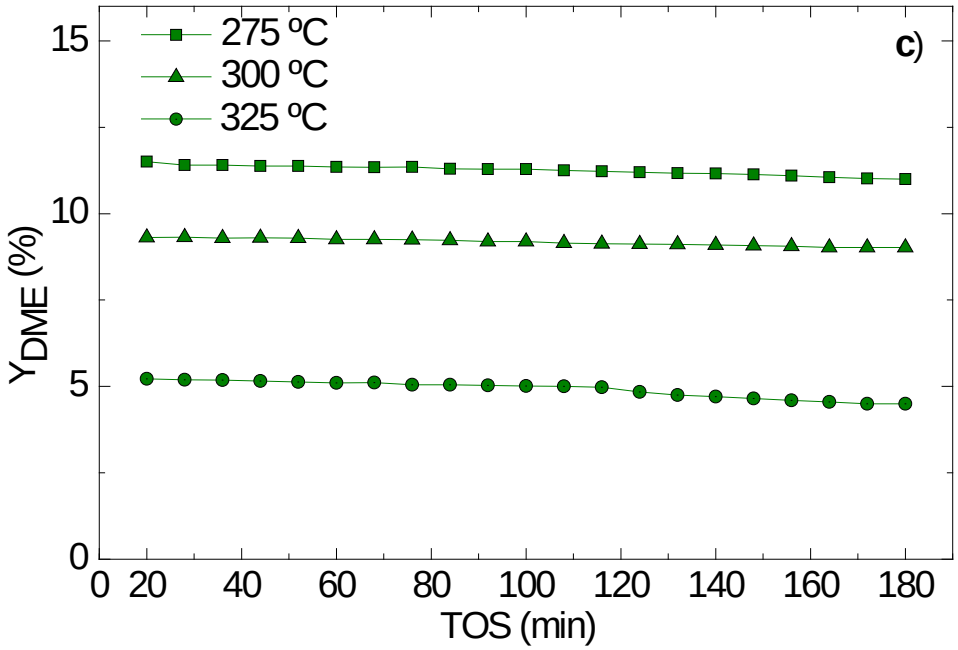

Fig. 7. Effect of reaction temperature on DME, MeOH and hydrocarbons yield, and CO_x and CO_2 conversion (a), on product selectivity (b) at zero time on stream; and the evolution of DME yield with time on stream (c) at different reaction temperatures. Reaction conditions: 40 bar; 10 g_{cat} h $(mol_C)^{-1}$; CO_2/CO_x, 1; H_2/CO, 3. Permeate conditions: equal composition and flow rate (60 cm^3 min^{-1}) as in the reaction section.

The aforementioned results obtained in PBMR reveal the capacity of this reactor for CO_2 conversion and also the significant effect of the CO_2 content in the feed on products conversion and yield. Comparing Figs. 6 and 7, the lower CO_x conversion and the lower DME yield and selectivity are remarkable feeding H_2+CO_2. This fact evidences the effect of increasing CO_2 content at the reactor inlet, which can also be observed feeding syngas (results not shown) obtaining greater results. Moreover, for H_2 +CO/CO_2 feeds (Fig. 6) CO_2 and CO_x conversions are enhanced increasing reaction temperature, whereas DME yield achieves its maximum at 300 ºC. Nevertheless, feeding H_2+CO_2 (Fig. 7), these indices diminish when increasing temperature, being

relevant the enhancement in CO_2 conversion, term related to the valorization of this compound. In this sense, a CO_2 conversion of 45 % achieved in one-pass feeding H_2+CO_2 at 325 ºC is an excellent result. On the other hand, although DME selectivity is lower for this feed, it must be pointed out that paraffins selectivity is inferior and that the higher methanol selectivity does not represent a major economic problem.

As it has also been indicated, catalyst deactivation is lower when incrementing CO_2 content in the feed, which is attributable to the fact that higher H_2O concentration in the reaction medium, generated by the WGS reaction, favors the attenuation of coke formation. This comparison, accordingly, indicates that PBMR is particularly attractive for feeds with high CO_2 concentration.

Given the possibility that the deactivation of the membrane may fade the deactivation of the catalyst, the experiments have been repeated replacing the catalyst by fresh catalyst. The results resulted to be the same as those shown in Fig. 7, revealing the stability of the membrane.

3.5. PBMR, Effect of pressure

In Fig. 8a the effect of pressure on the products yield at 300 ºC is depicted. The operating pressure has been found to have a notable effect on CO_x conversion at zero time on stream, rising paraffins, MeOH and DME yields practically linearly, which is due to the favorable effect of pressure on reactions with a reduction in the number of moles. Hence, increasing the pressure from 20 to 30 bar boosts CO_x conversion from 8.8 to 17.9 % and DME yield from 7.0 to 13.7 %. In spite of the positive effect of pressure on these reaction indices, further experiments with higher pressures have not

been carried out due to their asymptotic increasing tendency over 40 bar with packed bed reactors without membranes (Ereña et al., 2005; Jia et al., 2006; Behrens et al., 2012; Khoshbin and Haghighi, 2013; Azizi et al., 2014) and that operational issues may appear increasing the pressure.

As a result of the enhancement in all products yields, DME and MeOH selectivities remain constant within the studied pressure range (S_{DME} of 78 % and S_{MeOH} of 19 %) (Fig. 8b). Concerning paraffins selectivity, it rises from 1.82 to 4.47 % in the 20-40 bar range. Fig. 8c displays the role the operating pressure plays in catalyst stability. It is observed that under not severe conditions (20 bar), the evolution of DME yield with TOS is practically horizontal in 3 h. Increasing the operating pressure catalyst deactivation becomes more significant, being the most rapid at 40 bar and specially during the first hour of reaction.

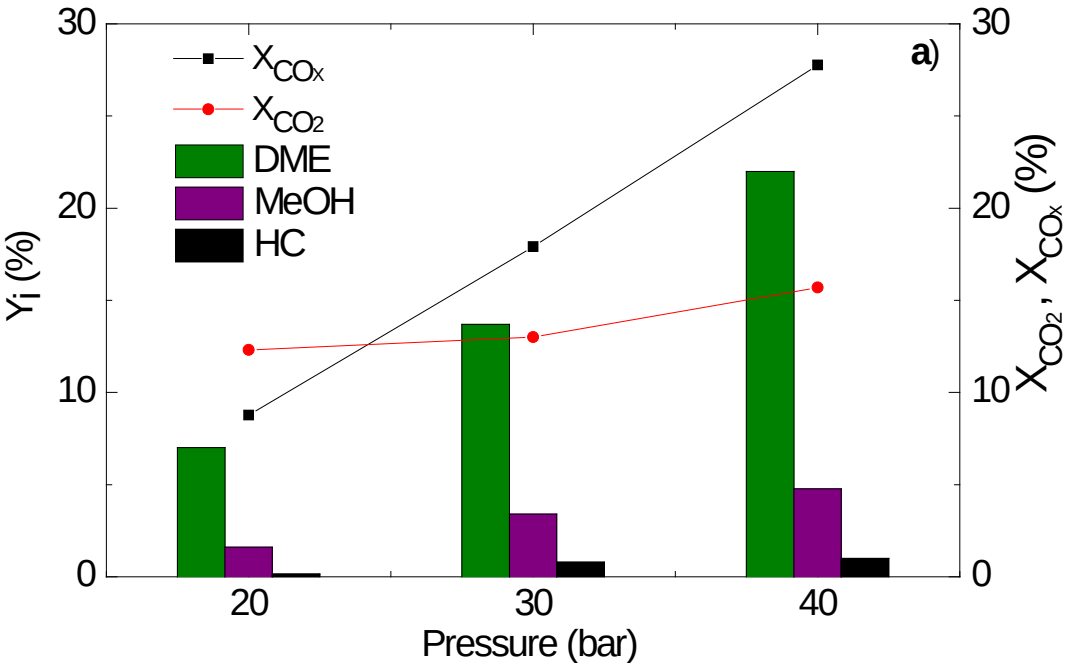

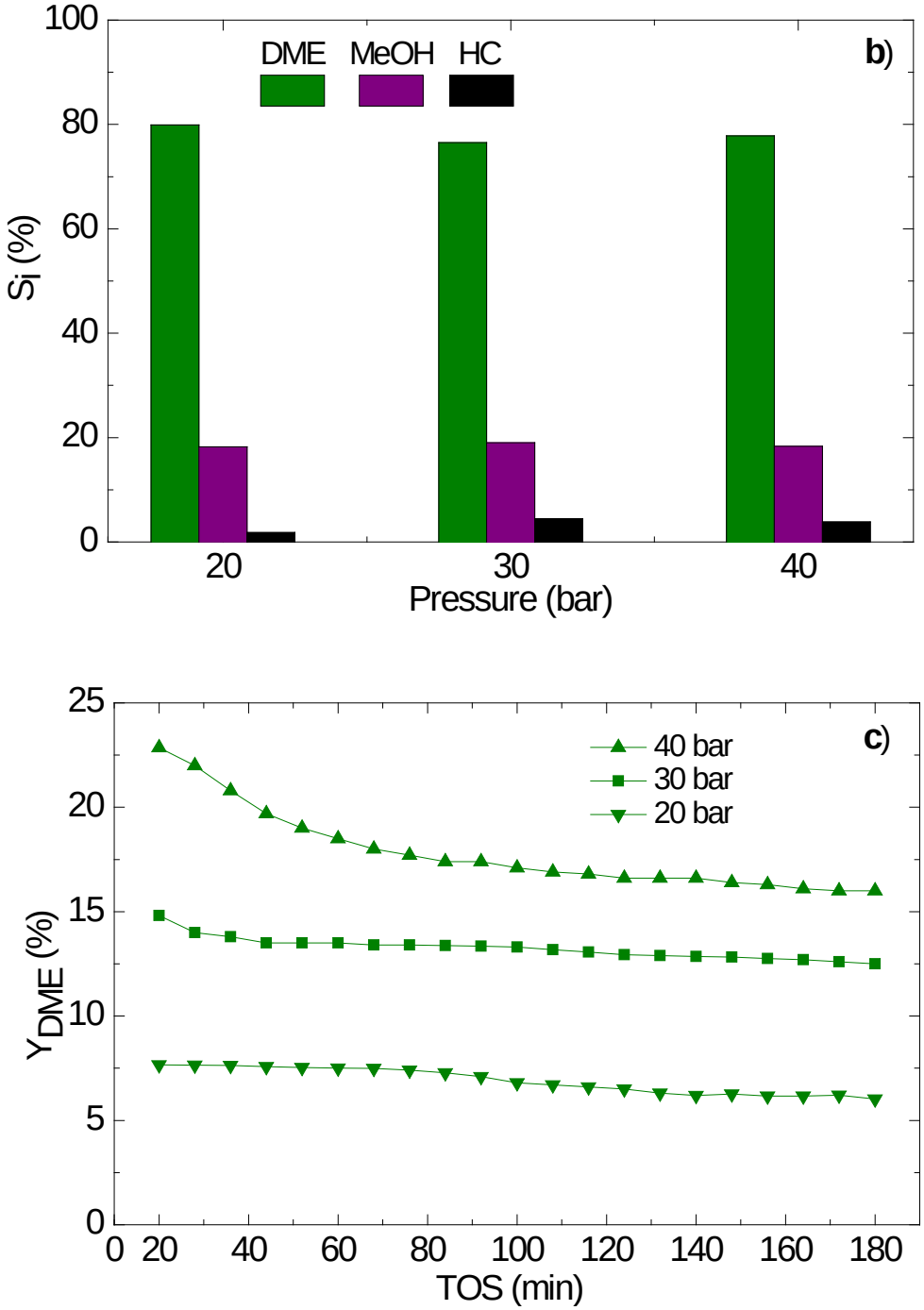

Fig. 8. Effect of pressure on DME, MeOH and hydrocarbons yield, and CO_x and CO_2 conversion (a) and on product selectivity (b) at zero time on stream; and the evolution of DME yield with time on stream at different reaction pressures (c). Reaction conditions: 300 º; 10 g_{cat} h $(mol_C)^{-1}$; CO_2/CO_x, 0.5; H_2/CO, 3. Permeate conditions: equal composition and flow rate (60 cm^3 min^{-1}) as in the reaction section.

The effect of pressure on the reaction indices feeding H_2+CO_2 has been studied at 275 ºC (Fig. 9). This temperature has been determined in Section 3.1 to be the most appropriate to achieve maximum DME yield with this feedstock. The increase of the operating pressure favors the linear rise of both CO_x conversion (from 3.0 to 14.9 %) and CO_2 conversion (from 9.4 to 25.0 %) within 10-40 bar range (Fig. 9a). Concerning DME and MeOH yields, the enhancement with pressure is clearly observed whereas paraffins formation remains quasi-negligible, achieving a maximum of 0.01 % under 40 bar. Due the constant rise of the products yield within the studied pressure range, MeOH and DME selectivity (Fig. 9b) are barely affected by the increase of the operating pressure (from 23.9 to 20.0 % and from 76.1 to 80.0 %, respectively). Fig. 9c displays the deactivation of the catalyst with time on stream. It demonstrates that, at this temperature and feeding H_2+CO_2, the deactivation of the catalyst is practically negligible throughout 3 h of reaction at the studied pressure range.

Attending to these results under different pressures, even though temperature is different for the two feeds, the effect of pressure for H_2+CO/CO_2 and H_2+CO_2 feeds is qualitatively similar. The drop of DME yield decreasing the pressure (interesting for reducing operating costs) is proportionally similar for both feeds, as well as the decay in CO_x conversion. Regarding DME selectivity, it is constant with pressure in both cases. Nonetheless, feeding syngas, a pressure decrease implies a rise of paraffins selectivity to the detriment of that of methanol (being favored CH_4 synthesis and Fischer-Tropsch reactions with respect to methanol synthesis). Feeding CO_2 at 275 ºC, on the contrary, paraffins formation is insignificant even under 10 bar. It is also remarkable that catalyst deactivation is slightly favored by the increase of pressure for syngas feeds at 325 ºC, and very slow for H_2 +CO_2 feeds at 275 ºC.

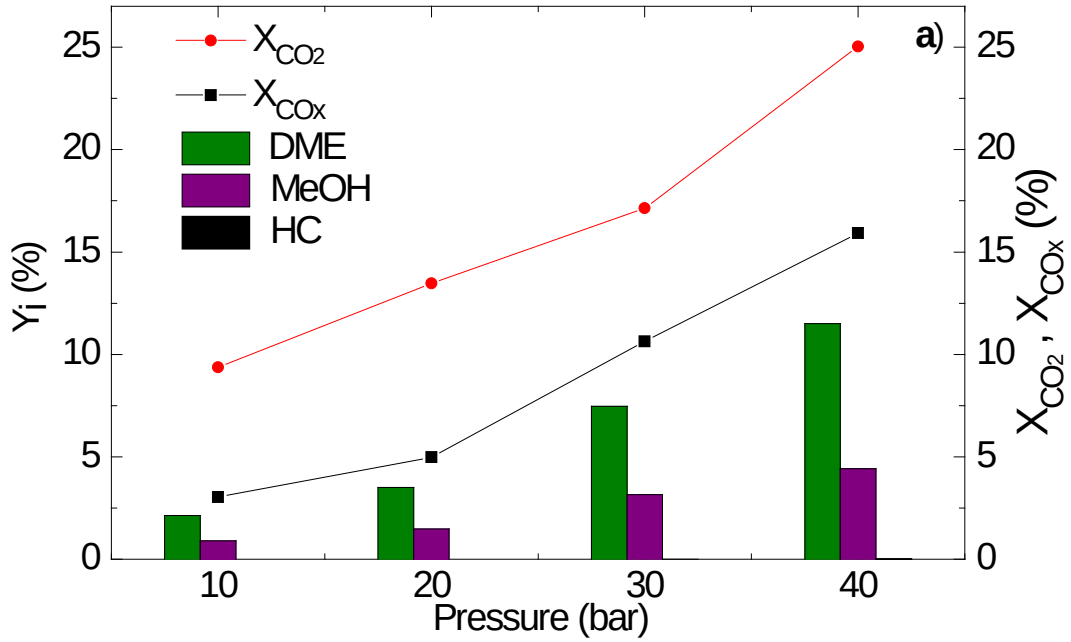
a)
X_{CO2}
X_{COx}
DME
MeOH
HC
Y_i (%)
X_{CO2} , X_{COx} (%)
Pressure (bar)
0
5
10
15
20
25
10
20
30
40

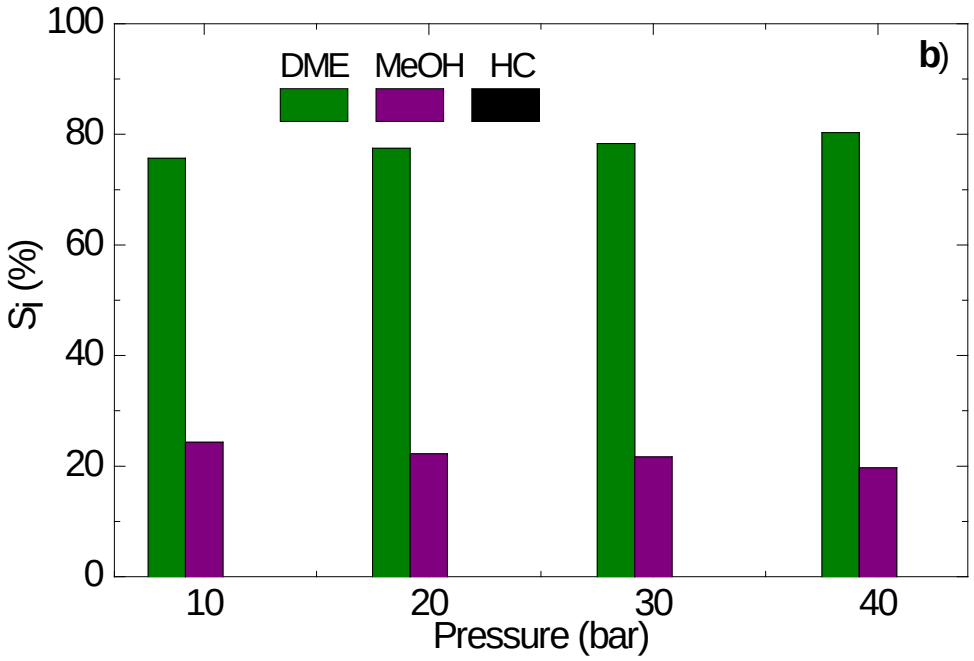
b)
DME
MeOH
HC
S_i (%)
Pressure (bar)
0
20
40
60
80
100
10
20
30
40

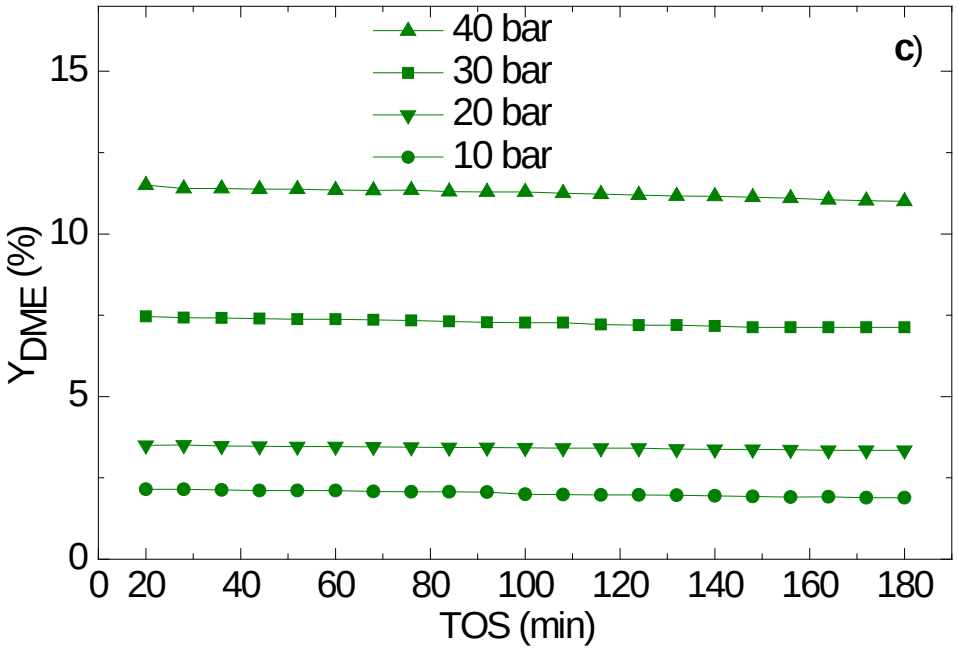

Fig. 9. Effect of pressure on DME, MeOH and hydrocarbons yield, and CO_x and CO_2 conversion (a) and on product selectivity (b) at zero time on stream; and the evolution of DME yield with time on stream at different pressures (c). Reaction conditions: 275 º; 10 g_{cat} h $(mol_C)^{-1}$; CO_2/CO_x, 1; H_2/CO, 3. Permeate conditions: equal composition and flow rate (60 cm^3 min^{-1}) as in the reaction section.

3.6. Comparison between PBMR and PBR

The elimination of H_2O from the reaction medium has two potential effects: i) the alteration of the theoretical thermodynamic equilibrium towards an apparent equilibrium, and ii) the increase of the reaction rate of some stages of the reaction. As aforementioned, according to the thermodynamics (Ateka et al., 2017), when CO_2 concentration in the feedstock increases, the thermodynamic limitations of the reaction augment, due to the increment of H_2O concentration in the reaction medium (formed by methanol synthesis (Eq. (2)) and rWGS (Eq. (3)) reactions). Besides, the H_2O is

adsorbed on the acid sites of the catalyst competing with the reactants and reducing its capacity to dehydrate methanol (Jun et al., 2002) on the one hand, and, on the other hand, on the metallic sites limiting the methanol synthesis rate (Dadgar et al., 2016).

Fig. 10 shows oxygenates yields (MeOH + DME) obtained for certain operating conditions at different temperatures. These results aim to verify how the removal of H_2O from the reaction medium using a PBMR permits overtaking the thermodynamic equilibrium of the process predicted for PBR (without membrane for H_2O removal). It can be observed that increasing temperature up to 325 ºC, the yield enhancement using a PBMR compared with the process thermodynamic equilibrium for PBR becomes more significant.

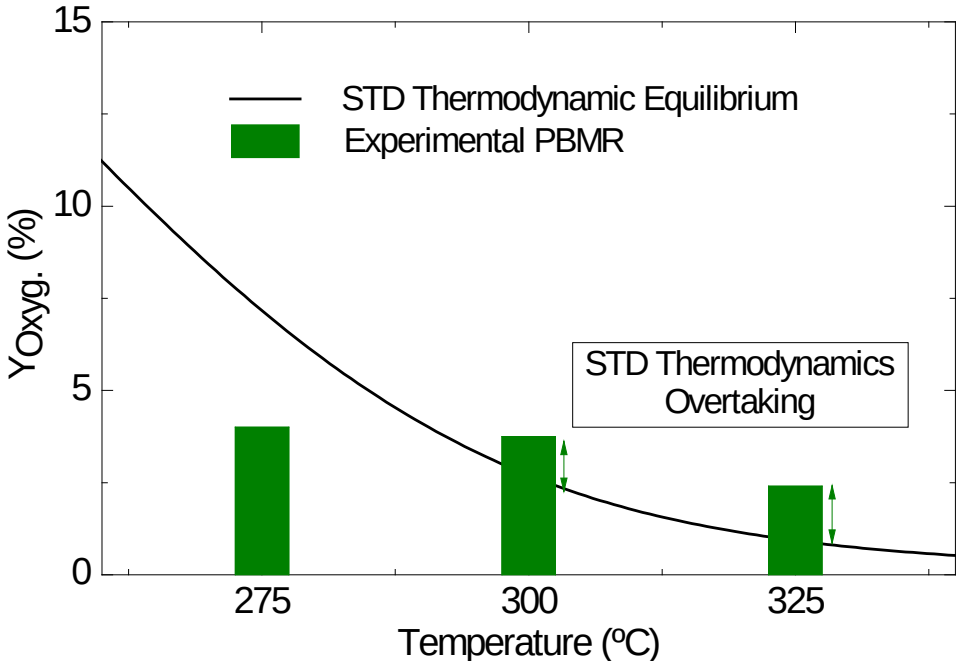

Fig. 10. Comparison of the experimental values of oxygenates yields obtained in PBMR with the thermodynamic equilibrium values predicted without membrane. Reaction conditions: 20 bar; 10 g_{cat} h $(mol_C)^{-1}$; CO_2/CO_x, 1; H_2/CO_x, 3. Permeate conditions for the PBMR: equal composition and flow rate (60 cm^3 min^{-1}) as in the reaction section.

For studying quantitatively the influence of incorporating a membrane on the yield of oxygenates and on CO_2 conversion Fig. 11 is presented. The comparison between oxygenates (DME and MeOH) yield evolution with temperature obtained in PBR and PBMR reactors feeding H_2+CO_2 is depicted in Fig. 11a. In all the cases, within the studied temperature range (275-325 ºC) and at 30 bar, oxygenates yield is enhanced using a PBMR. This improvement is greater when increasing temperature, from 2.80 to 6.57 % at 325 ºC. The conversion of CO_2 is also greater in the PBMR within the studied temperature range, observing the highest enhancement (37 %) at 325 ºC (Fig. 11b). The results in Figs. 10 and 11 highlight that in the operation in the PBMR, the separation of H_2O has a great effect on increasing the yield of oxygenates and CO_2 conversion. As a consequence of the partial separation of H_2O from the reaction medium, a pseudo-equilibrium state is reached, whose conversion also decreases with increasing temperature. In this pseudo-equilibrium, the decrease of limit conversion with rising temperature is attenuated with respect to the thermodynamics prediction.

Fig. 11c shows the effect of CO_2/CO_x ratio in the feed from 0 to 1 on oxygenates yield at 325 ºC. Higher yield is observed in PBMR whatever the CO_2 content in the feed. Being the most remarkable, the greatest upgrade obtained with the highest CO_2 content in the feed, improving oxygenates yield by 86 % when feeding H_2+CO_2.

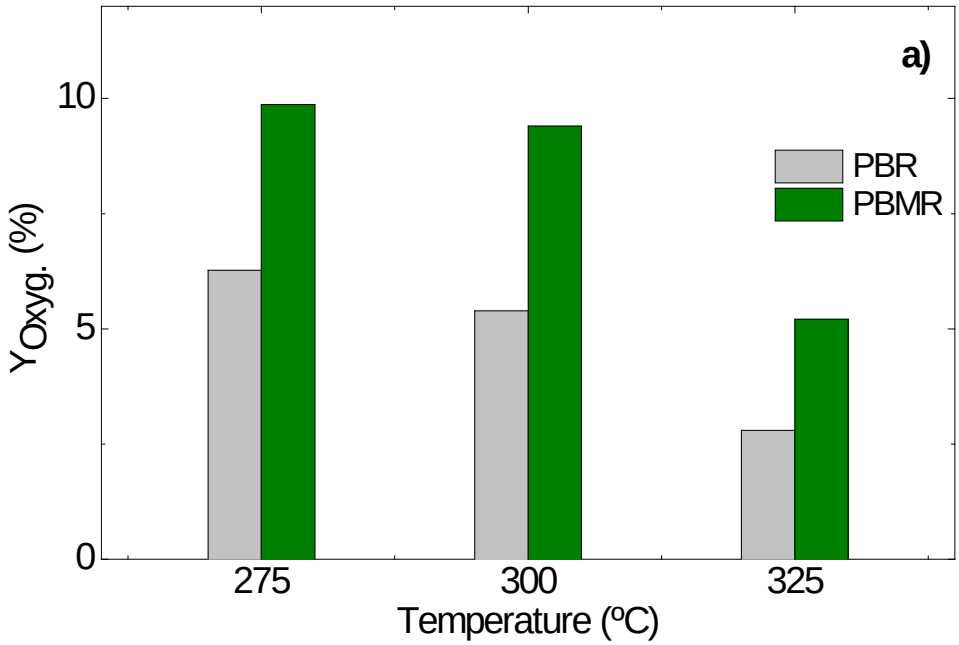
a)
PBR
PBMR
$Y_{Oxyg.}$ (%)
10
5
0
275
300
325
Temperature (ºC)

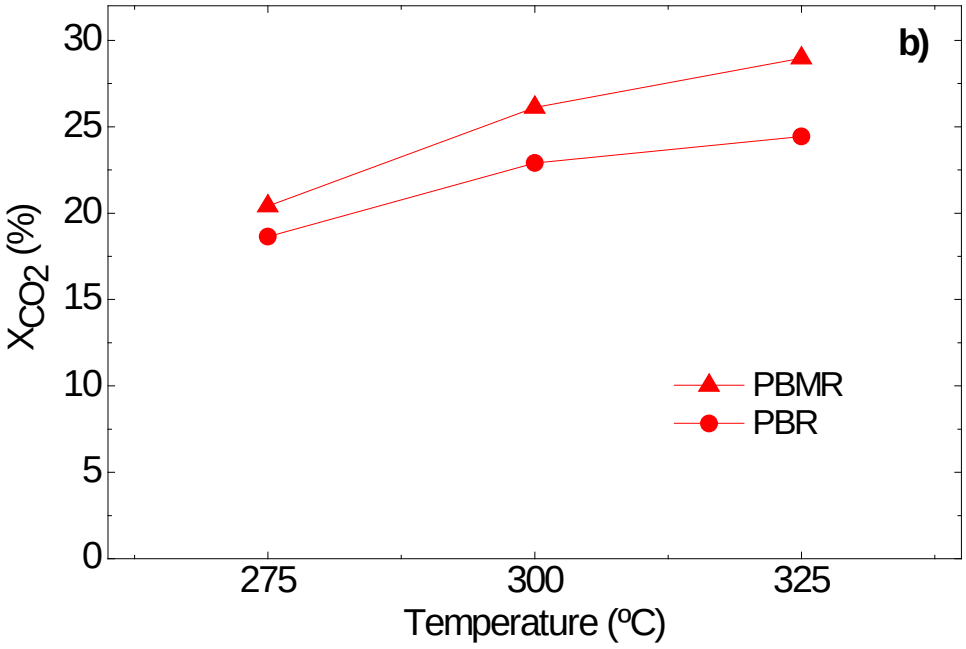
b)
PBMR
PBR
X_{CO2} (%)
30
25
20
15
10
5
0
275
300
325
Temperature (ºC)

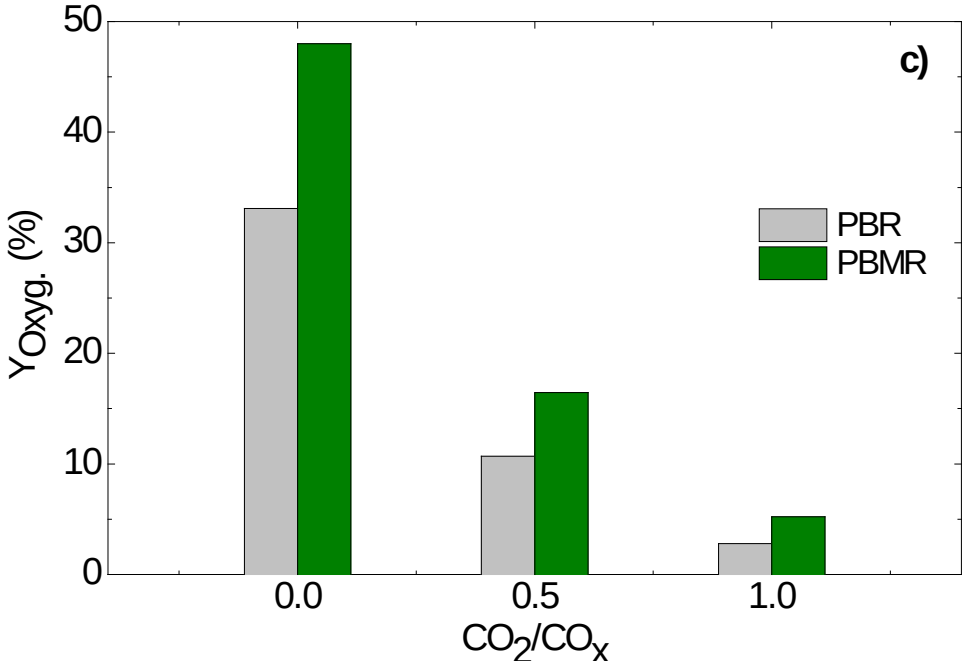

Fig. 11. Comparison of the PBMR and PBR. Oxygenates yield (a) and CO_2 conversion (b) at different temperatures; and oxygenates yield for different CO_2/CO_x ratios in the feed (c). Reaction conditions: 325 ºC; 30 bar; 10 g_{cat} h $(mol_C)^{-1}$; H_2/CO_x, 3; CO_2/CO_x, 1. Permeate conditions for the PBMR: equal composition and flow rate (60 cm^3 min^{-1}) as in the reaction section.

The effect of membrane utilization is more relevant with increasing space time. In Fig. 12, the yield of DME and the conversion of CO_2 at zero time on stream can be observed for different space time values. As it can be observed, the better performance of the PBMR over the PBR is greater upon increasing space time (industrially operating conditions). Indeed, for the studied conditions (325 ºC, 30 bar) and a H_2+CO_x feedstock with CO_2/CO_x= 0.5, using a membrane reactor doubles the yield of DME obtained with a PBR for a space time of 100 g h $(mol_C)^{-1}$, and boosts CO_2 conversion in a major extent. That is, at large-scale production conditions, thus, at high space time values, the

separation of H_2O from the reaction medium has a greater effect because it shifts the values of DME yield and CO_2 conversion with respect to the thermodynamic equilibrium in the PBR.

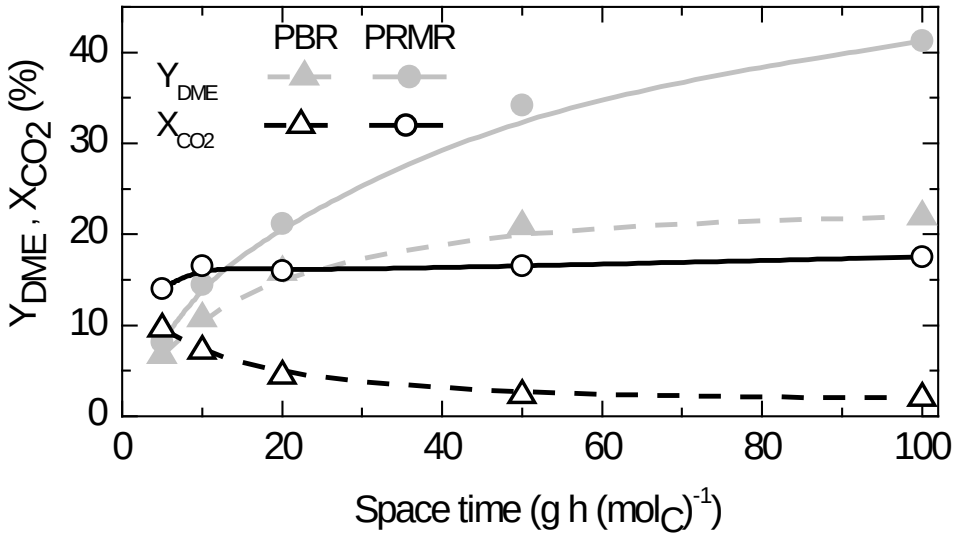

Fig. 12. Comparison of the evolution with space time of DME yield and CO_2 conversion in PBMR (continuous lines) and PBR (dashed lines). Reaction conditions: 325 ºC; 30 bar; H_2/CO_x, 3; CO_2/CO_x, 0.5.

Although the removal of H_2O from the reaction medium improves the reaction rates, it has an undesired side effect, because it is well established that the presence of H_2O in the reaction medium reduces coke formation. Sierra et al. (2011) explain this effect by the attenuation of the formation of methoxy ions from methanol and DME. It is also well established that these ions are the intermediates precursors of hydrocarbons formation in the acid function (Bjørgen et al., 2007). In addition, the greater capacity of DME for the formation of methoxy ions is considered to be the main cause of the higher rate of hydrocarbons and coke formation compared to that of methanol (Cordero-Lanzac

et al., 2018; Ibáñez et al., 2017). This effect has been studied by determining the coke content in the used catalysts by means of thermogravimetric analyses of their combustion with air. For the conditions in Fig. 12 and CO_2/CO_x = 0.5, coke content in 3 h is 0.32 wt% in the PBR and 0.61 wt% in the PBMR. This deposition of coke results in a partial deterioration of the properties of the catalyst. The textural, metallic and acid properties of the catalyst after its use under different reaction conditions have been gathered in Table A3. Consequently, and as expected, the removal of H_2O from the reaction medium has the unfavorable effect of upturning coke content. However, this effect is not very relevant and has little consequence in the evolution of the reaction indices with TOS. To explain this low incidence of H_2O separation on deactivation, it must be taken into account that the greater advance of the reaction in the PBMR also yields higher H_2O content. Thus, despite the separation, a sufficient H_2O concentration is present to limit the formation of coke. In addition, this problem is less relevant when feeding CO_2, since the formation of H_2O is favored and therefore, the attenuation of deactivation.

The stability of the aforementioned results has been experimentally ascertained by means of repeated runs with the same membrane. It should be noted that the results in this work correspond to per-pass conversions. Indeed, to assess the effect of the reaction variables in the performance of the catalyst, the study has been carried out under kinetic regime, ensuring there is no thermodynamic restrictions conditioning the results; enabling therefore the comparison of PBMR and PBR. The scaling up this process should be carried out recycling the nonconverted reactants (H_2, CO and CO_2) after the condensation of the oxygenates and H_2O. This recirculation strategy is used industrially in the synthesis of methanol (Bozzano and Manenti, 2016) and has also been proposed

for the direct synthesis of DME in conventional packed bed reactors (Ateka et al., 2020).

Conclusions

The partial elimination of H_2O from the reaction medium using an LTA zeolite membrane allows improving the results in the direct synthesis of DME with respect to the conventional (PBR) reactor. The obtained conversions are higher than those of the thermodynamic equilibrium for PBR and the decay of limit conversion when increasing temperature is limited with this strategy. This alteration of the equilibrium allows to achieve a DME yield of 14.8 % at 300 ºC co-feeding CO_2 with a CO_2/CO_x = 0.5 ratio in mild conditions (30 bar; space time, 10 g_{cat} h $(mol_C)^{-1}$; H_2/CO_x, 3) and with slow deactivation of the catalyst. Furthermore, the conversion of CO_2 under these conditions is of 14 %. For a relatively low temperature, 275 ºC, DME yield and CO_2 conversion are remarkable, of 11 and 12 %, respectively, whereas the formation of paraffins is insignificant and the deactivation is very slow.

The increase in pressure in the 10-40 bar range results in an almost linear increase in DME yield and CO_2 conversion, for both H_2+CO/CO_2 and H_2+CO_2 feeds. For the H_2+CO_2 feed, DME yield is lower than for H_2+CO/CO_2 feeds but CO_2 conversion is higher. Thus, for H_2+CO_2 feeds, 275 ºC (suitable temperature), 40 bar and space time of 10 g_{cat} h $(mol_C)^{-1}$, a DME yield of 12 % and a CO_2 conversion value of 20 % are attained, without paraffin formation and great catalyst stability. This stability is justified by the partial separation of H_2O from the reaction medium, which allows the reaction to be carried out at 325 ºC.

Acknowlegments

This work has been carried out with the financial support of the Ministry of Economy and Competitiveness of the Spanish Government (CTQ2016-77812-R), the Basque Government (Project IT1218-19), the ERDF funds and the European Commission (HORIZON H2020-MSCA RISE-2018. Contract No. 823745).

References

Aguayo, A.T., Ereña, J., Mier, D., Arandes, J.M., Olazar, M., Bilbao, J., 2007. Kinetic modeling of dimethyl ether synthesis in a single step on a CuO-ZnO-Al_2O_3/γ-Al_2O_3 catalyst. Ind. Eng. Chem. Res. 46, 5522–5530. https://doi.org/10.1021/ie070269s

Arcoumanis, C., Bae, C., Crookes, R., Kinoshita, E., 2008. The potential of di-methyl ether (DME) as an alternative fuel for compression-ignition engines: A review. Fuel 87, 1014–1030. https://doi.org/10.1016/j.fuel.2007.06.007

Ateka, A., Ereña, J., Bilbao, J., Aguayo, A.T., 2020. Strategies for the Intensification of CO_2 Valorization in the One-Step Dimethyl Ether Synthesis Process. Ind. Eng. Chem. Res. 59, 713–722. https://doi.org/10.1021/acs.iecr.9b05749

Ateka, A., Ereña, J., Bilbao, J., Aguayo, A.T., 2018. Kinetic modeling of the direct synthesis of dimethyl ether over a CuO‑ZnO‑MnO/SAPO‑18 catalyst and assessment of the CO_2 conversion. Fuel Process. Technol. 181, 233–243. https://doi.org/10.1016/j.fuproc.2018.09.024

Ateka, Ainara, Ereña, J., Pérez-Uriarte, P., Aguayo, A.T.A.T., Bilbao, J., 2017. Effect of the content of CO_2 and H_2 in the feed on the conversion of CO_2 in the direct synthesis of dimethyl ether over a CuO-ZnO-Al_2O_3/SAPO-18 catalyst. Int. J. Hydrogen Energy 42, 27130–27138. https://doi.org/https://doi.org/10.1016/j.ijhydene.2017.09.104

Ateka, A., Pérez-Uriarte, P., Gamero, M., Ereña, J., Aguayo, A.T., Bilbao, J., 2017. A comparative thermodynamic study on the CO_2 conversion in the synthesis of methanol and of DME. Energy 120, 796–804. https://doi.org/10.1016/j.energy.2016.11.129

Ateka, A., Sierra, I., Ereña, J., Bilbao, J., Aguayo, A.T., 2016. Performance of CuO–ZnO–ZrO_2 and CuO–ZnO–MnO as metallic functions and SAPO-18 as acid function of the catalyst for the synthesis of DME co-feeding CO_2. Fuel Process. Technol. 152, 34–45. https://doi.org/10.1016/j.fuproc.2016.05.041

Azizi, Z., Rezaeimanesh, M., Tohidian, T., Rahimpour, M.R., 2014. Dimethyl ether: A review of technologies and production challenges. Chem. Eng. Process. Process Intensif. 82, 150–172. https://doi.org/http://dx.doi.org/10.1016/j.cep.2014.06.007

Bedard, R., Liu, C., 2018. Recent Advances in Zeolitic Membranes. Annu. Rev. Mater. Res. 48, 83–110. https://doi.org/10.1146/annurev-matsci-070317-124605

Behrens, M., Studt, F., Kasatkin, I., Kühl, S., Hävecker, M., Abild-Pedersen, F., Zander, S., Girgsdies, F., Kurr, P., Kniep, B.L., Tovar, M., Fischer, R.W., Nørskov, J.K., Schlögl, R., 2012. The active site of methanol synthesis over Cu/ZnO/Al2O 3 industrial catalysts. Science 336, 893–897. https://doi.org/10.1126/science.1219831

Belviso, C., Lettino, A., Cavalcante, F., 2018. Influence of Synthesis Method on LTA Time-Dependent Stability. Molecules 23, 2122. https://doi.org/10.3390/molecules23092122

Bjørgen, M., Svelle, S., Joensen, F., Nerlov, J., Kolboe, S., Bonino, F., Palumbo, L.,

Bordiga, S., Olsbye, U., 2007. Conversion of methanol to hydrocarbons over zeolite H-ZSM-5: On the origin of the olefinic species. J. Catal. 249, 195–207. https://doi.org/10.1016/j.jcat.2007.04.006

Bonura, G., Cannilla, C., Frusteri, L., Catizzone, E., Todaro, S., Migliori, M., Giordano, G., Frusteri, F., 2020. Interaction effects between CuO-ZnO-ZrO_2 methanol phase and zeolite surface affecting stability of hybrid systems during one-step CO_2 hydrogenation to DME. Catal. Today 345, 175–182. https://doi.org/10.1016/j.cattod.2019.08.014

Bonura, G., Frusteri, F., Cannilla, C., Drago Ferrante, G., Aloise, A., Catizzone, E., Migliori, M., Giordano, G., 2016. Catalytic features of CuZnZr–zeolite hybrid systems for the direct CO_2-to-DME hydrogenation reaction. Catal. Today 277, 48–54. https://doi.org/10.1016/j.cattod.2016.02.013

Bozzano, G., Manenti, F., 2016. Efficient methanol synthesis: Perspectives, technologies and optimization strategies. Prog. Energy Combust. Sci. 56, 71-105. https://doi.org/10.1016/j.pecs.2016.06.001

Cai, M., Palčić, A., Subramanian, V., Moldovan, S., Ersen, O., Valtchev, V., Ordomsky, V. V, Khodakov, A.Y., 2016. Direct dimethyl ether synthesis from syngas on copper–zeolite hybrid catalysts with a wide range of zeolite particle sizes. J. Catal. 338, 227–238. https://doi.org/https://doi.org/10.1016/j.jcat.2016.02.025

Cannilla, C., Bonura, G., Frusteri, F., 2017. Potential of Pervaporation and Vapor Separation with Water Selective Membranes for an Optimized Production of Biofuels—A Review. Catalysts 7, 187–215. https://doi.org/10.3390/catal7060187

Catizzone, E., Bonura, G., Migliori, M., Frusteri, F., Giordano, G., 2018. CO_2 recycling to dimethyl ether: State-of-the-art and perspectives. Molecules 23, 31–59. https://doi.org/10.3390/molecules23010031

Chen, W.-H., Hsu, C.-L., Wang, X.-D., 2016. Thermodynamic approach and comparison of two-step and single step DME (dimethyl ether) syntheses with carbon dioxide utilization. Energy 109, 326–340. https://doi.org/10.1016/j.energy.2016.04.097

Cordero-Lanzac, T., Ateka, A., Pérez-Uriarte, P., Castaño, P., Aguayo, A.T., Bilbao, J., 2018. Insight into the Deactivation and Regeneration of HZSM-5 Zeolite Catalysts in the Conversion of Dimethyl Ether to Olefins. Ind. Eng. Chem. Res. 57, 13689–13702. https://doi.org/10.1021/acs.iecr.8b03308

Dadgar, F., Myrstad, R., Pfeifer, P., Holmen, A., Venvik, H.J., 2016. Direct dimethyl ether synthesis from synthesis gas: The influence of methanol dehydration on methanol synthesis reaction. Catal. Today 270, 76–84. https://doi.org/10.1016/j.cattod.2015.09.024

Database of Zeolite Structures [WWW Document], n.d. URL http://www.iza-structure.org/databases/ (accessed 11.23.20).

De Falco, M., Capocelli, M., Basile, A., 2017a. Selective membrane application for the industrial one-step DME production process fed by CO_2 rich streams: Modeling and simulation. Int. J. Hydrogen Energy 42, 6771–6786. https://doi.org/10.1016/j.ijhydene.2017.02.047

De Falco, M., Capocelli, M., Centi, G., 2016. Dimethyl ether production from CO_2 rich feedstocks in a one-step process: Thermodynamic evaluation and reactor simulation. Chem. Eng. J. 294, 400–409. https://doi.org/http://dx.doi.org/10.1016/j.cej.2016.03.009

De Falco, M., Capocelli, M., Giannattasio, A., 2017b. Membrane Reactor for one-step DME synthesis process: Industrial plant simulation and optimization. J. CO_2 Util. 22, 33–43. https://doi.org/10.1016/j.jcou.2017.09.008

Diban, N, Aguayo, A.T., Bilbao, J., Urtiaga, A., Ortiz, I., 2013. Membrane reactors for in situ water removal: A review of applications. Ind. Eng. Chem. Res. 52, 10342–10354. https://doi.org/10.1021/ie3029625

Diban, N., Urtiaga, A.M., Ortiz, I., Ereña, J., Bilbao, J., Aguayo, A.T., 2014. Improved performance of a pbm reactor for simultaneous CO_2 capture and DME synthesis. Ind. Eng. Chem. Res. 53, 19479–19487. https://doi.org/10.1021/ie503663h

Diban, Nazely, Urtiaga, A.M., Ortiz, I., Ereña, J., Bilbao, J., Aguayo, A.T., 2013. Influence of the membrane properties on the catalytic production of dimethyl ether with in situ water removal for the successful capture of CO_2. Chem. Eng. J. 234, 140–148. https://doi.org/10.1016/j.cej.2013.08.062

Ereña, J., Garoña, R., Arandes, J.M., Aguayo, A.T., Bilbao, J., 2005. Effect of operating conditions on the synthesis of dimethyl ether over a CuO-ZnO-Al_2O_3/NaHZSM-5 bifunctional catalyst. Catal. Today 107–108, 467–473. https://doi.org/10.1016/j.cattod.2005.07.116

Farsi, M., Hallaji Sani, A., Riasatian, P., 2016. Modeling and operability of DME production from syngas in a dual membrane reactor. Chem. Eng. Res. Des. 112, 190–198. https://doi.org/10.1016/j.cherd.2016.06.019

Farsi, M., Jahanmiri, A., 2012. Dynamic modeling of a H_2O-permselective membrane reactor to enhance methanol synthesis from syngas considering catalyst deactivation. J. Nat. Gas Chem. 21, 407–414. https://doi.org/10.1016/S1003-9953(11)60383-6

Fedosov, D.A., Smirnov, A. V., Shkirskiy, V. V., Voskoboynikov, T., Ivanova, I.I., 2015. Methanol dehydration in NaA zeolite membrane reactor. J. Memb. Sci. 486, 189–194. https://doi.org/10.1016/j.memsci.2015.03.047

Frusteri, F., Bonura, G., Cannilla, C., Drago Ferrante, G., Aloise, A., Catizzone, E., Migliori, M., Giordano, G., 2015. Stepwise tuning of metal-oxide and acid sites of CuZnZr-MFI hybrid catalysts for the direct DME synthesis by CO_2 hydrogenation. Appl. Catal. B Environ. 176–177, 522–531. https://doi.org/http://dx.doi.org/10.1016/j.apcatb.2015.04.032

Frusteri, F., Migliori, M., Cannilla, C., Frusteri, L., Catizzone, E., Aloise, A., Giordano, G., Bonura, G., 2017. Direct CO_2-to-DME hydrogenation reaction: New evidences of a superior behaviour of FER-based hybrid systems to obtain high DME yield. J. CO2 Util. 18, 353–361. https://doi.org/10.1016/j.jcou.2017.01.030

Gallucci, F., 2018. Inorganic Membrane Reactors for Methanol Synthesis, in: Methanol: Science and Engineering. Elsevier, pp. 493–518. https://doi.org/10.1016/B978-0-444-63903-5.00018-2

Gallucci, F., Paturzo, L., Basile, A., 2004. An experimental study of CO_2 hydrogenation into methanol involving a zeolite membrane reactor. Chem. Eng. Process. Process Intensif. 43, 1029–1036. https://doi.org/10.1016/j.cep.2003.10.005

García-Trenco, A., Martínez, A., 2012. Direct synthesis of DME from syngas on hybrid CuZnAl/ZSM-5 catalysts: New insights into the role of zeolite acidity. Appl. Catal. A Gen. 411–412, 170–179. https://doi.org/http://dx.doi.org/10.1016/j.apcata.2011.10.036

García-Trenco, A., Vidal-Moya, A., Martínez, A., 2012. Study of the interaction between components in hybrid CuZnAl/HZSM-5 catalysts and its impact in the syngas-to-DME reaction. Catal. Today 179, 43–51. https://doi.org/http://dx.doi.org/10.1016/j.cattod.2011.06.034

Good, D.A., Francisco, J.S., 2003. Atmospheric Chemistry of Alternative Fuels and Alternative Chlorofluorocarbons. Chem. Rev. 103, 4999–5023. https://doi.org/10.1021/cr020654l

Gorbe, J., Lasobras, J., Francés, E., Herguido, J., Menéndez, M., Kumakiri, I., Kita, H., 2018. Preliminary study on the feasibility of using a zeolite A membrane in a membrane reactor for methanol production. Sep. Purif. Technol. 200, 164–168. https://doi.org/10.1016/j.seppur.2018.02.036

Ibáñez, M., Pérez-Uriarte, P., Sánchez-Contador, M., Cordero-Lanzac, T., Aguayo, A.T., Bilbao, J., Castaño, P., 2017. Nature and Location of Carbonaceous Species in a Composite HZSM-5 Zeolite Catalyst during the Conversion of Dimethyl Ether into Light Olefins. Catalysts 7, 254–266. https://doi.org/10.3390/catal7090254

Iliuta, I., Iliuta, M.C., Larachi, F., 2011. Sorption-enhanced dimethyl ether synthesis-Multiscale reactor modeling. Chem. Eng. Sci. 66, 2241–2251. https://doi.org/10.1016/j.ces.2011.02.047

Iliuta, I., Larachi, F., Fongarland, P., 2010. Dimethyl ether synthesis with in situ H_2O removal in fixed-bed membrane reactor: Model and simulations. Ind. Eng. Chem. Res. 49, 6870–6877. https://doi.org/10.1021/ie901726u

Javanmard, H., Seyyedi, M., Jones, S.A., Nielsen, S.M., 2019. Dimethyl Ether Enhanced Oil Recovery in Fractured Reservoirs and Aspects of Phase Behavior. Energy & Fuels 33, 10718–10727. https://doi.org/10.1021/acs.energyfuels.9b02600

Jia, G., Tan, Y., Han, Y., 2006. A Comparative Study on the Thermodynamics of Dimethyl Ether Synthesis from CO Hydrogenation and CO_2 Hydrogenation. Ind. Eng. Chem. Res. 45, 1152–1159. https://doi.org/10.1021/ie050499b

Jun, K.W., Lee, H.S., Roh, H.S., Park, S.E., 2002. Catalytic dehydration of methanol to dimethyl ether (DME) over solid-acid catalysts. Bull. Korean Chem. Soc. 23, 803–806. https://doi.org/10.5012/bkcs.2002.23.6.803

Khoshbin, R., Haghighi, M., 2013. Direct syngas to DME as a clean fuel: The beneficial use of ultrasound for the preparation of CuO-ZnO-Al_2O_3/HZSM-5 nanocatalyst. Chem. Eng. Res. Des. 91, 1111–1122. https://doi.org/10.1016/j.cherd.2012.11.017

Lee, J., Park, H.G., Hyeon, M.H., Kim, B.G., Kim, S.K., Moon, S.Y., 2021. Low-temperature CO_2 hydrogenation overcoming equilibrium limitations with

polyimide hollow fiber membrane reactor. Chem. Eng. J. 403, 126457–126466. https://doi.org/10.1016/j.cej.2020.126457

Leonzio, G., 2018. State of art and perspectives about the production of methanol, dimethyl ether and syngas by carbon dioxide hydrogenation. J. CO2 Util. 27, 326–354. https://doi.org/10.1016/j.jcou.2018.08.005

Mondal, U., Yadav, G.D., 2019. Perspective of dimethyl ether as fuel: Part I. Catalysis. J. CO2 Util. 32, 299–320. https://doi.org/10.1016/j.jcou.2019.02.003

Oar-Arteta, L., Remiro, A., Epron, F., Bion, N., Aguayo, A.T., Bilbao, J., Gayubo, A.G., 2016. Comparison of Noble Metal- and Copper-Based Catalysts for the Step of Methanol Steam Reforming in the Dimethyl Ether Steam Reforming Process. Ind. Eng. Chem. Res. 55, 3546–3555. https://doi.org/10.1021/acs.iecr.6b00126

Olah, G.A., Goeppert, A., Prakash, G.K.S., 2009. Chemical recycling of carbon dioxide to methanol and dimethyl ether: From greenhouse gas to renewable, environmentally carbon neutral fuels and synthetic hydrocarbons. J. Org. Chem. 74, 487–498. https://doi.org/10.1021/jo801260f

Osatiashtiani, A., Puértolas, B., Oliveira, C.C.S., Manayil, J.C., Barbero, B., Isaacs, M., Michailof, C., Heracleous, E., Pérez-Ramírez, J., Lee, A.F., Wilson, K., 2017. On the influence of Si:Al ratio and hierarchical porosity of FAU zeolites in solid acid catalysed esterification pretreatment of bio-oil. Biomass Convers. Biorefinery 7, 331–342. https://doi.org/10.1007/s13399-017-0254-x

Perez-Carbajo, J., Balestra, S.R.G., Calero, S., Merkling, P.J., 2020. Effect of lattice shrinking on the migration of water within zeolite LTA. Microporous Mesoporous Mater. 293, 109808. https://doi.org/10.1016/j.micromeso.2019.109808

Pérez-Uriarte, P., Ateka, A., Aguayo, A.T., Gayubo, A.G., Bilbao, J., 2016. Kinetic model for the reaction of DME to olefins over a HZSM-5 zeolite catalyst. Chem. Eng. J. 302, 801–810. https://doi.org/10.1016/j.cej.2016.05.096

Rafiee, A., Rajab Khalilpour, K., Milani, D., Panahi, M., 2018. Trends in CO_2 conversion and utilization: A review from process systems perspective. J. Environ. Chem. Eng. 6, 5771–5794. https://doi.org/10.1016/j.jece.2018.08.065

Sánchez-Contador, M., Ateka, A., Aguayo, A.T., Bilbao, J., 2018a. Direct synthesis of dimethyl ether from CO and CO_2 over a core-shell structured CuO-ZnO-ZrO_2@SAPO-11 catalyst. Fuel Process. Technol. 179, 258–268. https://doi.org/10.1016/j.fuproc.2018.07.009

Sánchez-Contador, M., Ateka, A., Aguayo, A.T., Bilbao, J., 2018b. Behavior of SAPO-11 as acid function in the direct synthesis of dimethyl ether from syngas and CO_2. J. Ind. Eng. Chem. 63, 245–254. https://doi.org/10.1016/j.jiec.2018.02.022

Sánchez-Contador, M., Ateka, A., Rodriguez-Vega, P., Bilbao, J., Aguayo, A.T., 2018c. Optimization of the Zr Content in the CuO-ZnO-ZrO_2/SAPO-11 Catalyst for the Selective Hydrogenation of CO+CO_2 Mixtures in the Direct Synthesis of Dimethyl Ether. Ind. Eng. Chem. Res. 57, 1169–1178. https://doi.org/10.1021/acs.iecr.7b04345

Semelsberger, T.A., Borup, R.L., Greene, H.L., 2006. Dimethyl ether (DME) as an alternative fuel. J. Power Sources 156, 497–511.

https://doi.org/10.1016/j.jpowsour.2005.05.082

Shimoda, N., Faungnawakij, K., Kikuchi, R., Eguchi, K., 2011. A study of various zeolites and $CuFe_2O_4$ spinel composite catalysts in steam reforming and hydrolysis of dimethyl ether. Int. J. Hydrogen Energy 36, 1433–1441. https://doi.org/http://dx.doi.org/10.1016/j.ijhydene.2010.10.088

Sierra, I., Ereña, J., Aguayo, A.T., Arandes, J.M., Olazar, M., Bilbao, J., 2011. Co-feeding water to attenuate deactivation of the catalyst metallic function (CuO–ZnO–Al_2O_3) by coke in the direct synthesis of dimethyl ether. Appl. Catal. B Environ. 106, 167–173. https://doi.org/http://dx.doi.org/10.1016/j.apcatb.2011.05.021

Sierra, I., Ereña, J., Aguayo, A.T., Ateka, A., Bilbao, J., 2013. Kinetic modelling for the dehydration of methanol to dimethyl ether over γ-Al_2O_3. Chem. Eng. Trans. 32, 613–618. https://doi.org/10.3303/cet1332103

Sun, J., Yang, G., Yoneyama, Y., Tsubaki, N., 2014. Catalysis chemistry of dimethyl ether synthesis. ACS Catal. 4, 3346–3356. https://doi.org/10.1021/cs500967j

Tian, Y., Demirel, S.E., Hasan, M.M.F., Pistikopoulos, E.N., 2018. An overview of process systems engineering approaches for process intensification: State of the art. Chem. Eng. Process. - Process Intensif. 133, 160-210. https://doi.org/10.1016/j.cep.2018.07.014

Zhou, X., Su, T., Jiang, Y., Qin, Z., Ji, H., Guo, Z., 2016. CuO-Fe_2O_3-CeO_2/HZSM-5 bifunctional catalyst hydrogenated CO_2 for enhanced dimethyl ether synthesis. Chem. Eng. Sci. 153, 10–20. https://doi.org/https://doi.org/10.1016/j.ces.2016.07.007